The Impact of Topography on the Environment and Life Cycle of Weakly and Strongly Forced MCSs during RELAMPAGO

MARQUETTE N. ROCQUE[a] AND KRISTEN L. RASMUSSEN[a]

[a] *Department of Atmospheric Science, Colorado State University, Fort Collins, Colorado*

(Manuscript received 21 February 2022, in final form 10 June 2022)

ABSTRACT: Intense deep convection and large mesoscale convective systems (MCSs) are known to occur downstream of the Andes in subtropical South America. Deep convection is often focused along the Sierras de Córdoba (SDC) in the afternoon and then rapidly grows upscale and moves to the east overnight. However, how the Andes and SDC impact the life cycle of MCSs under varying synoptic conditions is not well understood. Two sets of terrain-modification experiments using WRF are used to investigate the impact of topography in different synoptic regimes. The first set is run on the 13–14 December 2018 MCS case from RELAMPAGO, which featured a deep synoptic trough, strong lee cyclogenesis near the SDC, an enhanced low-level jet, and rapid upscale growth of an MCS. When the Andes are reduced by 50%, the lee cyclone and low-level jet that develop are weaker than with the full Andes, and the resulting MCS is weak and moves faster to the east. When the SDC are removed, few differences between the environment and resulting MCS relative to the control run are seen. A second set of experiments are run on the 25–26 January 2019 case in which a large MCS developed over the SDC and remained tied there for an extended period under weak synoptic forcing. The experiment that produces the most similar MCS to the control is when the Andes are reduced by 50% while maintaining the height of the SDC, suggesting the SDC may play a more important role in the MCS life cycle under quiescent synoptic conditions.

KEYWORDS: South America; Synoptic-scale processes; Mesoscale systems; Orographic effects; Mountain meteorology

1. Introduction

Global satellite studies have shown that some of the most intense deep convection occurs in the vicinity of large mountain ranges including the Rockies, Himalayas, and Andes (Zipser et al. 2006; Houze et al. 2015). It is hypothesized that these mountain ranges modulate the flow and environment in such a way that creates favorable conditions for the frequent development of mesoscale convective systems (MCSs). MCSs play an important role in the water and energy cycles through their influence on the radiation budget, and their vertical transport of latent heat and momentum (Houze 2004). Thus, better understanding the environments in which they form in around the world will aid in their representation in numerical weather forecasts and climate models.

In the past decade, specific focus has been given to subtropical South America (SSA) where Tropical Rainfall Measuring Mission (TRMM; Kummerow et al. 1998) satellite studies have shown a high frequency of deep convection with high lightning flash rates in all seasons, but especially in the spring and summer months (Zipser et al. 2006; Nesbitt et al. 2006; Romatschke and Houze 2010; Rasmussen and Houze 2011; Houze et al. 2015; Rasmussen et al. 2014, 2016). Nesbitt et al. (2006) found that MCSs contribute about 90% to the total rainfall in the La Plata basin in SSA, while other regions around the world including the Sahel, Congo basin, and the U.S. Great Plains have MCS rainfall contributions greater than 70%. Rasmussen et al. (2016) similarly found that nearly 95% of the warm-season rainfall over the eastern plains of Argentina comes from MCSs, and Liu and Zipser (2013) showed that the largest and strongest convective lines occur over central Africa, the southeastern United States, and Argentina. These large MCSs in SSA are often associated with severe weather including flooding, large hail, and tornadoes (Rasmussen and Houze 2011; Rasmussen et al. 2014; Bruick et al. 2019).

Using observations from TRMM and several model simulations, Rasmussen and Houze (2016; hereinafter RH16) investigated the impact of terrain on MCSs in SSA. They performed a variety of terrain-modification experiments that involved both reducing the height of the Andes and increasing the height of the southern Andes. They found that lowering the Andes resulted in a weaker South American low-level jet (SALLJ; Vera et al. 2006; Sasaki et al. 2022), less convective available potential energy (CAPE) and convective inhibition (CIN), and more widespread convection that moved faster toward the east. Increasing the southern Andes resulted in a stronger SALLJ, more CAPE and CIN, and convection that was located farther south. These results

Corresponding author: Marquette N. Rocque, marquette.rocque@colostate.edu

DOI: 10.1175/MWR-D-22-0049.1

were used to develop a conceptual model of the important environmental conditions that support the production of large convective events in SSA (RH16). Warm, moist air transported from the Amazon basin to SSA along the SALLJ is capped by dry midlevel flow subsiding off the Andes. The northerly SALLJ then collides with southerly ageostrophic flow from the midlatitudes near the north–south-oriented Sierras de Córdoba (SDC) mountain range in western Argentina where deep convection is often initiated. Because of the extreme height of the Andes, CAPE and CIN are enhanced downstream of the topography relative to shorter mountain ranges. These conditions create a favorable environment for deep convection and rapid upscale growth that is focused along the topography.

Subsequent studies have followed this conceptual model and shown that some of the most intense convective features and severe weather are associated with these strong synoptic conditions including a deep upper-level trough, strong lee cyclogenesis, and an enhanced SALLJ. Piersante et al. (2021) analyzed 16 years of wide convective cores (40 dBZ echoes $>$ 1000 km^2; WCCs) identified by TRMM and found that large (>90% percentile) WCCs occurred under stronger synoptic conditions during the spring than during the summer. Additionally, small (<10% percentile) WCCs occurred under quiescent synoptic flow in the summer. They suggested that the poleward and westward shift in upper-level troughs and jet streaks allowed convection to focus along the SDC in the summer, helping to explain the westward shift in WCC rainfall observed by Rasmussen et al. (2016). In terms of severe weather, Bruick et al. (2019) found that systems with a high probability of hail occurred under more anomalous synoptic conditions.

Because of the polar-orbiting nature of TRMM and the lack of ground-based radar observations in SSA until 2015, the complete life cycle of MCSs and how they evolve within the large-scale flow has not been studied in great detail. This was a primary motivation for the Remote Sensing of Electrification, Lightning, And Mesoscale/Microscale Processes with Adaptive Ground Observations (RELAMPAGO; Nesbitt et al. 2021) field campaign, which took place near Córdoba, Argentina, in late 2018–early 2019. Several studies have used resulting datasets from RELAMPAGO and the Córdoba radar to investigate how intense convective events are related to the large-scale flow in SSA. A recent study by Sasaki et al. (2022) used sounding observations from RELAMPAGO to analyze the relationship between SALLJ events and convection in the region and found that longer-duration jets were often more elevated, associated with large precipitation events, and driven by the synoptic flow, where lee cyclogenesis intensifies the north–south pressure gradient force downstream of the Andes. Shorter-duration jets were controlled by the diurnal cycle (Holton 1967) and boundary layer processes such as the inertial oscillation (Blackadar 1957), more similar to jets in the U.S. Great Plains (Du and Rotunno 2014; Shapiro et al. 2016).

Using two years of data from the Córdoba radar, Mulholland et al. (2018) produced one of the first studies on the convective life cycle within the SSA region. They found that the majority of convective events near the SDC were multicellular in nature, initiated over the highest terrain of the southern SDC, and often rapidly grew upscale directly downstream of the SDC in as little as three hours. These events were associated with deep upper-level troughs, a strong SALLJ, and enhanced CAPE and CIN, further supporting RH16's conceptual model. Further studies by Mulholland et al. (2019, 2020) looked at varying the height of the SDC and the resulting changes to the environment and convective development/evolution. Results from their case study analysis (Mulholland et al. 2019), as well as idealized simulations (Mulholland et al. 2020), show that increasing the SDC height increases vertical wind shear, reduces CAPE, leads to convection initiating earlier, and causes enhanced blocking of cold pools. The deepest cold pools and fastest transition from supercell to MCS occurred in the control run, suggesting the SDC are at a unique height for intense and rapid upscale growth (Mulholland et al. 2019). However, the influence of the synoptic environment was not considered, especially in the idealized simulations. Interestingly, Parker (2021) has recently shown that nocturnal MCSs in the U.S. Great Plains can have a considerable self-organizing component in which the evolution of the MCS is dependent on its own environment and prior evolution. They find the synoptic scale provides a favorable environment for MCS initiation, but mesoscale dynamics associated with the MCS such as cold pool processes ultimately control the MCS life cycle.

As mentioned, there are a lot of ingredients that come together to create a favorable environment for MCS development in SSA (RH16). It is known that the Andes and SDC play a major role in modulating the environment, but there has been little research on terrain influences on the environment and convection under different (particularly weak) synoptic conditions associated with the development and upscale growth of MCSs in the region. Several of the studies mentioned above have shown that large MCSs, often associated with severe weather, tend to occur under strong synoptic conditions in the spring, yet results from RELAMPAGO demonstrate that MCSs occur under a range of synoptic environments in SSA. Thus, the main objective of this study is to explore how the Andes and SDC impact the environment and convective development under strong and weak synoptic conditions in SSA.

2. Methodology

a. *Model*

The impact of the Andes and the SDC on convective growth is analyzed using a set of five terrain-modification experiments. The Weather Research and Forecasting (WRF; Skamarock et al. 2008) Model, version 4.2, was run to simulate two cases from the RELAMPAGO field campaign. The first is an upscale growth MCS case that occurred on 13–14 December 2018 (IOP17) and resulted in large hail, significant lightning activity, and flooding. This case featured a deep upper-level trough and strong SALLJ and will be referred to as the strongly forced case. The second case is an upscale growth MCS event that occurred on 25–26 January 2019 and again resulted in significant severe weather associated with very deep convective cells with 40-dBZ echo tops greater than 20 km (Schumacher et al. 2021;

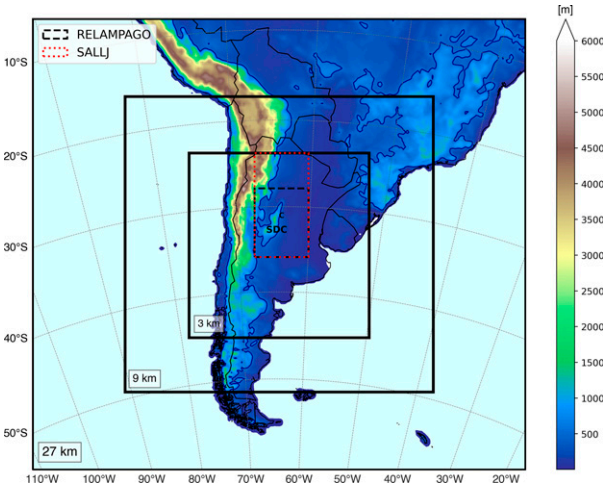

FIG. 1. The 27-, 9-, and 3-km domains used in the WRF simulations. The SALLJ domain (red dotted box) and RELAMPAGO domain (black dashed box) are used for Hovmöller averaging. CTRL topography is shaded, with the 500-m terrain contour in navy; the "C" represents Córdoba.

Nesbitt et al. 2021). A small upper-level short-wave trough passed through the midlatitudes but the flow across the Córdoba region was weakly zonal. Hence, this case will be referred to as the weakly forced case and provides a nice contrast to the strongly forced case. Both cases were initialized about 24 h before convection associated with the event of interest initiated (1800 UTC 12 December 2018 for the strongly forced case and 1800 UTC 24 January 2019 for the weakly forced case) and run for 54 h using three nested domains of 27, 9, and 3 km centered around Córdoba, Argentina (Fig. 1). ERA5 reanalysis data (Copernicus Climate Change Service 2017) were used to force the simulations every hour. The Thompson aerosol-aware microphysics scheme (Thompson and Eidhammer 2014) was used as it best represents both the convective and stratiform components of MCSs in SSA (RH16). Both sets of simulations used the following physics parameterizations: Rapid Radiative Transfer Model (RRTM) longwave radiation (Mlawer et al. 1997), Dudhia shortwave radiation (Dudhia 1989), Kain–Fritsch cumulus convection in the 27- and 9-km domains (none in the 3-km domain; Kain and Fritsch 1993), Monin–Obukhov surface layer scheme, Noah land surface model (Chen and Dudhia 2001), and the Yonsei University (YSU) planetary boundary layer (PBL) scheme (Hong et al. 2006).

The first simulation run for each case was the control (CTRL), in which the terrain in each domain was not altered. In the second simulation, the SDC were removed from each domain (noSDC; Fig. 2a). This was accomplished by creating several boxes over the SDC, setting the values inside each box to the average height of the terrain downstream of the SDC (60–100 m), and then using a 9-point smoothing function around the edge of the boxes to eliminate any sharp gradients in terrain that would have been produced. This was performed on each domain prior to running metgrid.exe, and the SDC-modification box domains are shown in Table 1. The third and fourth simulations involved reducing the height of the Andes by 50% and either keeping the SDC at the same height (lAndes; Fig. 2b) or removing them (lAndes_noSDC; Fig. 2c). Similar smoothing functions were applied near the modifications to create a more gradual slope. These experiments were designed to investigate how the height of the Andes impacts convective growth and synoptic to mesoscale flow features, and this terrain height more closely resembles the height of the Rockies in North America. For the final simulation, the terrain was completely removed across each domain (noTer; Fig. 2d). Results from this simulation highlight the important impact of the Andes, Andean foothills, and SDC on the development of intense MCSs in SSA. RH16 used this same method to modify terrain in their study (both the Andes and SDC modification), thus the current method is consistent with prior research.

b. GOES-16

Data from the *Geostationary Operational Environmental Satellite (GOES-16)* Advanced Baseline Imager (ABI; Schmit et al. 2017) were used to see how well the simulations captured the events. Here we use the channel-14 11.2-μm band (infrared longwave window) to look at cloud-top brightness temperatures.

c. ERA5

ERA5 reanalysis data (Copernicus Climate Change Service 2017), which have 0.25° × 0.25° resolution, 37 vertical grid levels, and hourly temporal resolution, were also used to examine the synoptic setup of the two cases. Relative vorticity at 500 hPa, specific humidity at 850 hPa, and geopotential height and winds at both 500 and 850 hPa were analyzed across South America. In addition, to look at the climatology of moisture in the region, the average monthly 850-hPa specific humidity was calculated for December and January from 1978 to 2018.

3. 13–14 December 2018: Strongly forced case

a. Overview

An intense MCS rapidly developed on the east side of the Andes in SSA during the RELAMPAGO field campaign from 13 to 14 December 2018 and was associated with strong synoptic forcing including a high-amplitude, slow-moving 500-hPa trough, strong lee cyclogenesis, and an enhanced low-level jet (Fig. 3). At 0000 UTC 13 December, an upper-level trough was located at 85°W off the coast of Chile (Fig. 3a). Enhanced moisture (>12 g kg^{-1}) was funneled along the eastern edge of the Andes from the Amazon to about 35°S at 850 hPa by the SALLJ (Fig. 3b). Over the next 24 h, the 500-hPa trough deepened as it approached the Andes, with the 552-dam height contour extending to around 38°S (Fig. 3c). Strong relative vorticity advection occurred downstream of the trough associated with both shear and curvature vorticity (Fig. 3c). At 850 hPa, the SALLJ increased in strength to −18 m s^{-1}, which advected specific humidity values of 10 g kg^{-1} to nearly 40°S (Fig. 3d). By 15 December, the 500- and 850-hPa troughs had moved over the Atlantic and the greatest moisture was

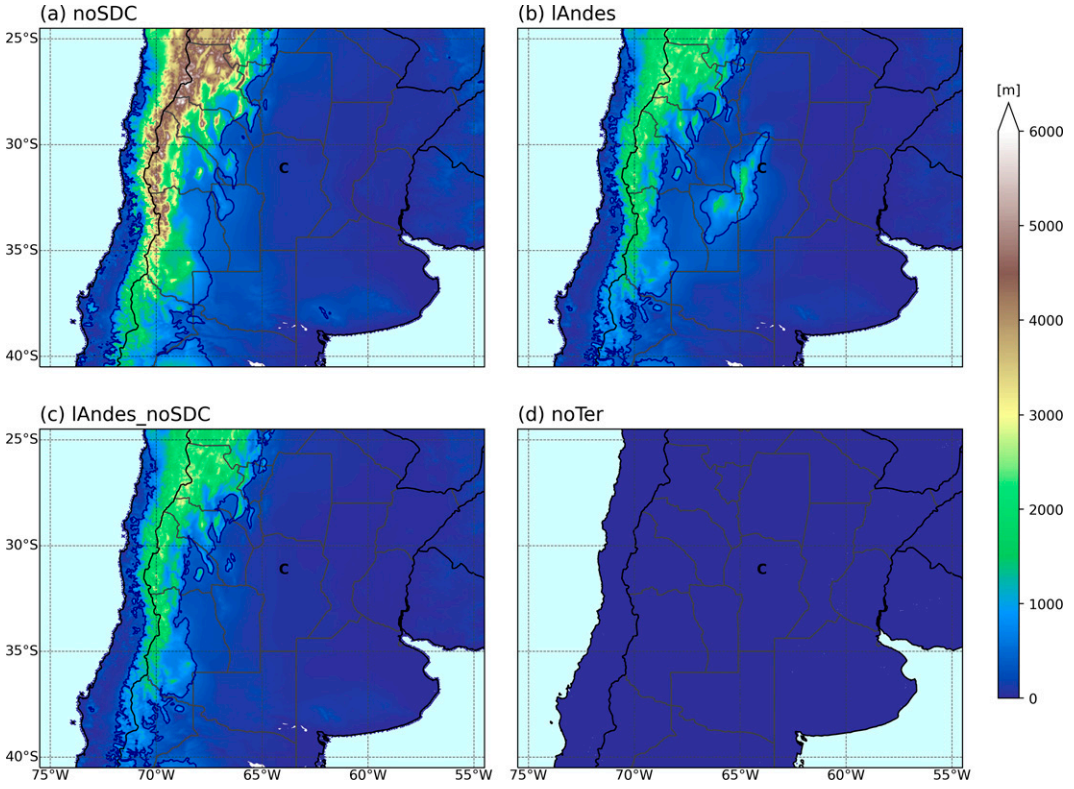

FIG. 2. Topography from the (a) noSDC, (b) lAndes, (c) lAndes_noSDC, and (d) noTer 3-km WRF simulations, with the 500-m terrain contour shown in navy; the "C" represents Córdoba.

concentrated north of the SDC and within the trough to the east (Figs. 3e,f).

Convective cells initiated around 1800 UTC 13 December on the southern end of the SDC and about three hours later off the higher terrain of the foothills to the north. After 0000 UTC 14 December, deep cells had developed south of Córdoba and over the southern SDC. These cells quickly grew into a strong convective line that remained tied to the Andes and SDC through 0600 UTC. A comparison between *GOES-16* infrared brightness temperatures and outgoing longwave radiation from the 3-km CTRL run shows that weaker convection was present over the eastern plains of Argentina from a previous system at 1200 UTC 13 December (Figs. 4a,b). Six hours later, convection initiated in similar locations near the SDC (Figs. 4c,d). The CTRL run is more aggressive in developing convection along the cold front to the south (Figs. 4c–f), but by 0600 UTC when the MCS reached peak maturity, the convective structures are quite similar (Figs. 4g,h). Therefore, we reason that the simulations provide valuable insight into the interactions between the topography and convective growth in the region.

b. *Synoptic scale*

Under strong synoptic conditions, the Andes act as a barrier to the upper-level flow (RH16). Figure 5a shows the progression of the 500-hPa trough in the CTRL run in a time–longitude (Hovmöller) format. The 500-hPa geopotential heights are averaged across the 3-km-domain latitude band (23°–45°S; Fig. 1) to examine the evolution of the upper-level flow in the subtropics that directly impacted the life cycle of the MCS. The trough is strongest on the west side of the Andes around 0900 UTC 13 December at 5565 m (Fig. 5a). As the trough approaches the Andes, it significantly weakens. When the Andes are reduced by 50%, the upper-level trough is at least 20 m (on average) deeper than the trough in the CTRL simulation (Fig. 5b) and is at least 40 m deeper when the terrain is removed completely (Fig. 5c). In the presence of the full Andes, the trough is sheared apart, but

TABLE 1. Summary of WRF domains and where SDC-modification boxes were placed within each domain. The last column is the height set within the terrain-modification box (approximately the height downstream of the SDC).

Name	Resolution	Grid points	Box 1	Box 2	Box 3	Height
d01	27 km	238 × 218	[111:121, 105:131]	—	—	60 m
d02	9 km	446 × 428	[214:240, 204:282]	[207:224, 207:263]	[198:216, 203:243]	100 m
d03	3 km	782 × 803	[370:435, 357:610]	[343:379, 356:559]	[316:345, 356:491]	100 m

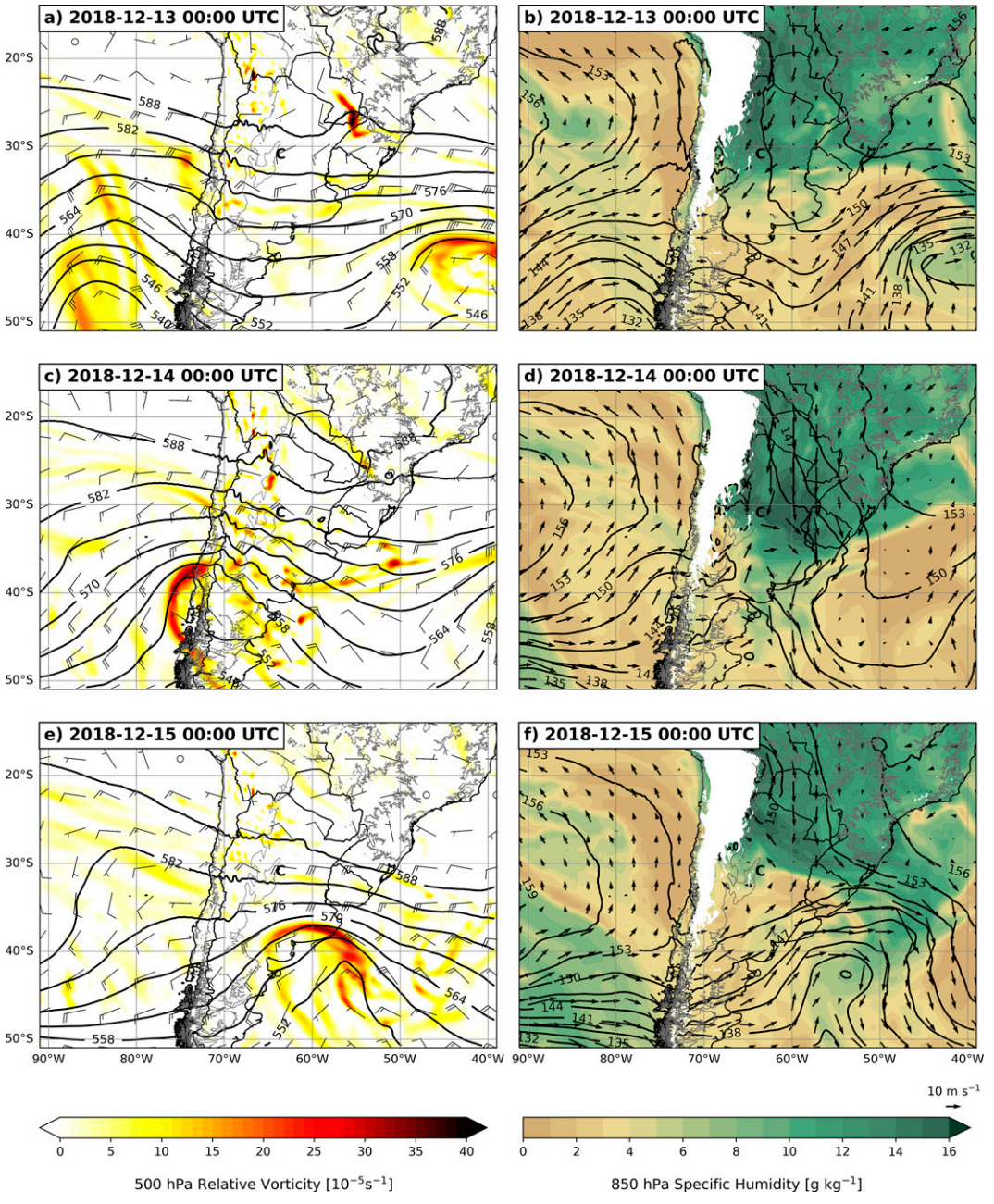

FIG. 3. (a),(c),(e) The 500-hPa geopotential heights (contoured; dam), relative vorticity (shaded; 10^{-5} s^{-1}), and winds (barbs; m s^{-1}, where a half barb is 5 m s^{-1} and a full barb is 10 m s^{-1}) and (b),(d),(f) 850-hPa geopotential heights (contoured; dam), specific humidity (shaded; g kg^{-1}), and winds (arrows; m s^{-1}) from ERA5 reanalysis starting at 0000 UTC 13 Dec 2018 and stepping through every 24 h. The 500-m terrain contour is shown in gray, and the "C" represents Córdoba.

when the Andes are reduced or removed, the upper-level flow remains intact and strong.

A lee cyclone develops downstream of the Andes in the CTRL run as a result of the strong upper-level trough and potential vorticity conservation, which is clearly visible at 1800 UTC 13 December, where the 1410- and 1425-m 850-hPa geopotential height contours are located near the SDC (Fig. 6a). There is a weaker signature of a lee cyclone when the Andes are reduced (Fig. 6b), but the main baroclinic system to the south is at least 30 m deeper. When the terrain is reduced/removed, the mechanism for producing a lee cyclone is also reduced/removed, so the only low pressure is associated directly with the upper-level trough in the midlatitudes (Figs. 6b,c). There is a small short wave visible in the noTer geopotential heights that could be a

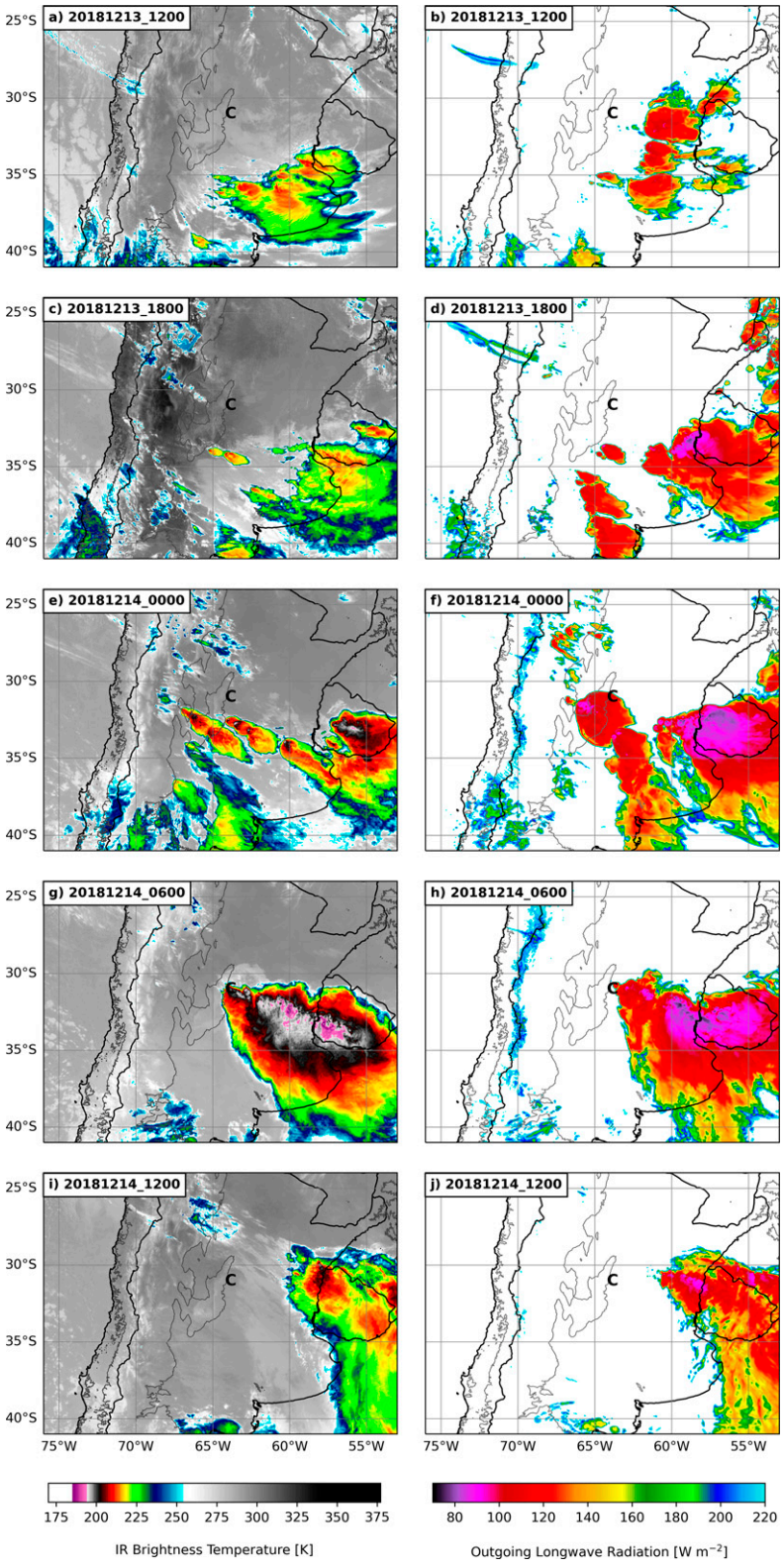

FIG. 4. (a),(c),(e),(g),(i) Comparison between *GOES-16* channel-14 IR brightness temperatures (K) and (b),(d),(f),(h),(j) outgoing longwave radiation from the 3-km CTRL run (W m^{-2}) starting at 1200 UTC 13 Dec 2018 and stepping through every 6 h. The 500-m terrain contour is shown in gray, and the "C" represents Córdoba.

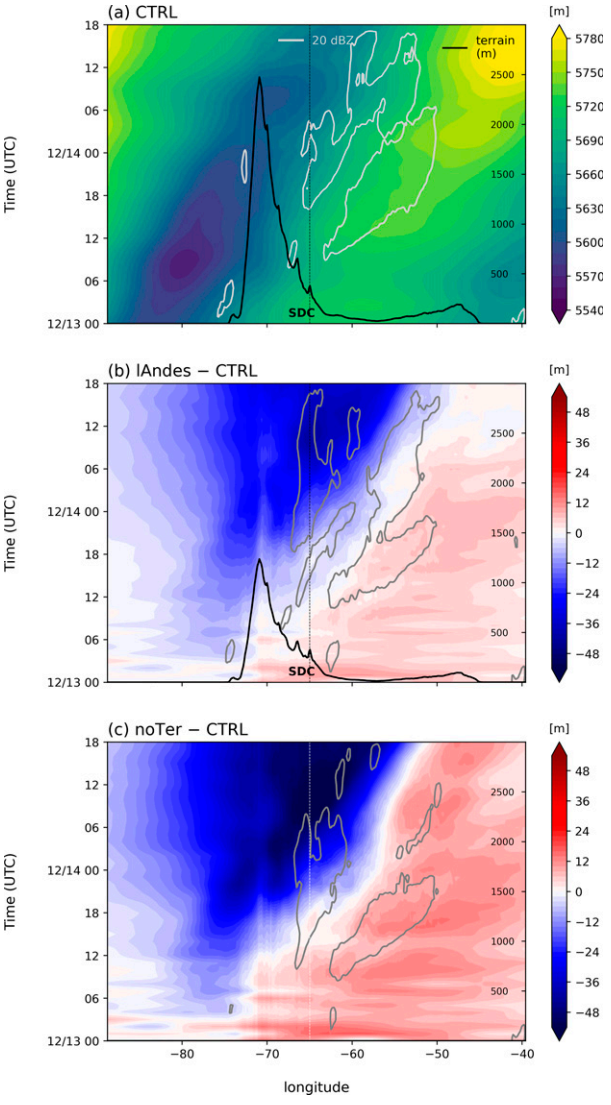

FIG. 5. Hovmöller diagrams of (a) CTRL 500-hPa heights (shaded; m) and 20-dBZ composite reflectivity (gray contour; dBZ) from the 9-km domain averaged across the 3-km-domain latitude band, (b) lAndes − CTRL, and (c) noTer − CTRL. Longitude ranges from about 90° to 40°W, and times are shown from 0000 UTC 13 to 1800 UTC 14 Dec. The average terrain profile is shown with the black contour. The location of the SDC near 65°W is shown as a dashed black line in (a) and (b), and where the SDC would be is shown as a dashed white line in (c).

forcing for new convection, but the mechanism for its production is not clear (Fig. 6c). The evolution of the 850-hPa geopotential heights averaged across the SALLJ domain (Fig. 1) in a Hovmöller format also highlights the development of the lee cyclone in the CTRL run (Fig. 7a). Geopotential heights are lowest between 1800 and 0000 UTC, and the minimum of 1390 m extends just east of the SDC. At this time, convection is initiated along the Andean foothills around 66.5°W and propagates east. When the Andes are halved, geopotential heights are at least 30 m greater between 1800 and 0000 UTC in the western part of the domain indicating a weaker cyclone, and there is little-to-no convection in this region (Fig. 7b). The cyclone is even weaker when the Andes are removed, with 850-hPa heights at least 60 m greater than the CTRL (Fig. 7c), again highlighting the impact of terrain height on lee cyclogenesis and convective development. RH16 similarly found that reducing the height of the Andes by 50% led to a significant increase in 850-hPa geopotential heights and weaker lee cyclogenesis close to the Andean foothills.

The movement of air parcels at different levels is also analyzed to better understand how the Andes impact the low-, mid-, and upper-level flow. Backward trajectories starting from 0000 UTC 14 December at a location north of the SDC (28.6°S, 63.5°W) are shown in Fig. 8. These trajectories were computed every 10 min in the Read/Interpolate/Plot (RIP) program maintained by the National Center for Atmospheric Research. Locations near Córdoba and Villa Yacanto, Argentina, within the SDC were also analyzed, but the influence of the SDC made results more difficult to interpret. This northern location was chosen because it is near the center of the SALLJ domain yet about 100 km north of the SDC. At 500 hPa, the trajectories of air parcels in each simulation are very similar (Fig. 8a). The 500-hPa flow in the CTRL simulation (red) is slower than in the lAndes (blue) and noTer (yellow) runs, though. At 1200 UTC 13 December, the 500-hPa parcels are located off the Chilean coast around 71°W in the lAndes and noTer runs, whereas the CTRL 500-hPa parcel is over the high terrain of the Andes (4400 m) near 69°W. There is not much vertical motion along the parcel trajectories as they all remained around 500 hPa (Fig. 8d). At 700 hPa, the trajectories are more unique for each terrain-modification experiment. The flow in the CTRL run originates over the eastern Andes (3100 m) at around 600 hPa and descends off the terrain to the southeast (Figs. 8b,e). As the height of the Andes decreases in each modification, the trajectories become more westerly and faster (Fig. 8b). There is also not much vertical motion with the lAndes and noTer 700-hPa parcels (Fig. 8e). At 850 hPa, the CTRL and lAndes runs both highlight the presence of the SALLJ (Fig. 8c). The average magnitude of the jet in the CTRL run is 17 m s^{-1}, whereas it is about 10 m s^{-1} in the lAndes run and has a more easterly component. There is no SALLJ signature in the noTer run because the SALLJ is partially driven by sloping terrain. Instead, the flow is weaker and generally from the west, demonstrating the clear role of the Andes in the low-level jet dynamics associated with the SALLJ (Vera et al. 2006; Insel et al. 2010; Sasaki et al. 2022).

Results from this analysis show how the Andes impact the synoptic environment in SSA. In the full-Andes simulations, the 500-hPa trough is strongest over the Chilean coast before becoming sheared apart by the Andes. A strong lee cyclone develops on the east side of the Andes in the subtropics that coincides with convection initiation. A strong SALLJ is present, which is likely strengthened by the north–south pressure gradient force induced by the lee cyclone. When the Andes are reduced by 50%, the upper-level trough crosses the Andes without being sheared apart, the resulting lee cyclone is significantly weaker, and the SALLJ, although still present, is nearly twice as slow as in the full-Andes case. When the

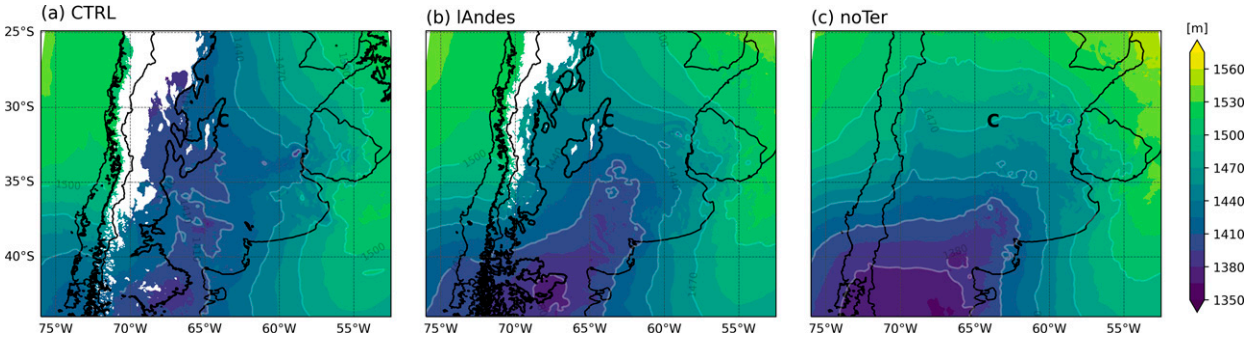

FIG. 6. The 850-hPa heights (m) from 1800 UTC 13 Dec for (a) CTRL, (b) lAndes, and (c) noTer simulations shown across the 3-km domain. The 500-m terrain contour is shown in black, and the "C" represents Córdoba.

Andes are removed completely, the upper-level trough steadily moves across southern South America, there is no lee cyclogenesis, and there is no low-level jet signature, consistent with previous studies on SALLJ dynamics (Marengo et al. 2004; Vera et al. 2006; Insel et al. 2010; Sasaki et al. 2022). The SALLJ characteristics will be further explored in the following section.

c. *SALLJ*

Two major components of the SALLJ are analyzed here: meridional flow and moisture. Although there is no cohesive hypothesis for moisture advection associated with the SALLJ in SSA like there is in the United States, several studies have shown that at least 20% of the moisture associated with warm-season precipitation over the La Plata basin in SSA comes from the southern Amazon via the SALLJ (Dirmeyer et al. 2009; Martinez and Dominguez 2014; Sasaki et al. 2022). Differences between the SALLJ across terrain-modification experiments are more closely examined with Hovmöller plots of 850-hPa meridional winds and specific humidity. The evolution of meridional winds across the SALLJ domain in the full Andes runs shows two maxima in northerly winds at 850 hPa at around -20 m s^{-1} (Figs. 9a,b). Both maxima extend from the eastern edge of the SDC to the eastern edge of the domain (60°W). The first occurs around 1300 UTC 13 December and has some convection associated with it, although mostly to the east of the SDC. The second maximum is connected to the large MCS event and is visible at 0000–0300 UTC 14 December. These results agree with Sasaki et al. (2022) who identified a low-level jet in consecutive soundings from Córdoba and Villa de María del Río Seco (~175 km north-northeast of Córdoba) from 0000 UTC 13 to 0600 UTC 14 December. After 0000 UTC, there is southerly flow over the higher terrain in both CTRL and noSDC cases. Some convection develops in this flow in the CTRL run but convection is mostly cut off in this transition zone in the noSDC run. In the lower Andes cases, the secondary northerly wind maximum disappears and winds across the entire domain are generally ~4–5 m s^{-1} weaker (Figs. 9c,d). No convection develops in the southerly flow. Once again, when the terrain is removed there is a single northerly wind maximum earlier in the period at 1200 UTC associated with convection to the east (Fig. 9e).

To put this event into context of the climatology, anomalies of specific humidity are calculated using the ERA5 December monthly means from 1978 to 2018 over the SALLJ domain. The average 850-hPa specific humidity value across the domain during December is 8.9 g kg^{-1}. This value is subtracted from the specific humidity values calculated in each WRF experiment to examine anomalous moisture in each simulation. In the CTRL run, the specific humidity anomaly is maximized at 8.1 g kg^{-1} around 1800 UTC directly downstream of the SDC and remains present until 0000 UTC (Fig. 10a). Convection initiates over the higher terrain of the Andes while this high moisture anomaly is present in the immediate lee of the Andes. When the SDC are removed, the moisture anomaly maximum is slightly weaker (~7.6 g kg^{-1}) and shorter lived relative to the CTRL (Fig. 10b). Convection initiates farther west along the Andes foothills in the noSDC case, but there is no evidence of repeated initiation later in the period. When the Andes are reduced by 50%, there is no longer a moisture maximum along the foothills (Figs. 10c,d). Instead, specific humidity is maximized east of 64°W. Anomalously dry air begins to enter the domain around 1800 UTC and remains over the Andes through the end of the period. This dry air likely inhibits convection from developing off the Andes and corresponds to the shift in winds (Figs. 9c,d). There are few differences between the lAndes and lAndes_noSDC runs, suggesting that the Andes have a larger impact than the SDC on convective development in this case, as was also shown in RH16. When the terrain is removed completely, dry air quickly spreads east, and any convection that does develop is confined to anomalously moist regions only (Fig. 10e).

These results are also visible when looking at a map of 850-hPa specific humidity and winds at 2100 UTC 13 December (Fig. 11). In the full Andes runs (CTRL and noSDC), the greatest moisture (>15 g kg^{-1}) is confined to the eastern edge of the Andes and downstream of the SDC region north of 33°S (Figs. 11a,b). Winds are strong from the north northeast at around -15 m s^{-1} in both simulations. There are very slight differences between the two, with moisture extending farther south in the CTRL run and winds about 5 m s^{-1} stronger directly downstream of the SDC relative to the noSDC

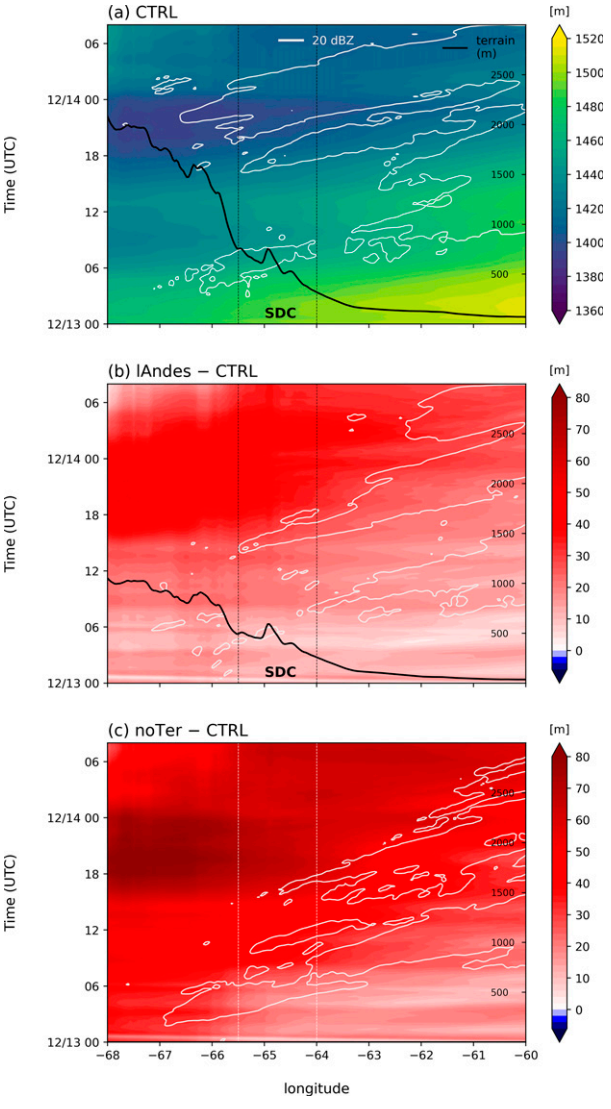

FIG. 7. Hovmöller diagrams of (a) CTRL 850-hPa heights (shaded; m) from the 3-km domain averaged across the SALLJ domain and 20-dBZ composite reflectivity (gray contour; dBZ) from the 3-km domain averaged across the RELAMPAGO domain, (b) lAndes − CTRL, and (c) noTer − CTRL. Longitude ranges from about 68° to 60°W, and times are shown from 0000 UTC 13 to 0800 UTC 14 Dec. The average terrain profile from the 3-km domain averaged across the SALLJ domain is shown with the black contour. The location of the SDC is shown within the dashed black lines in (a) and,(b), and where the SDC would be is shown within the dashed white lines in (c).

run. When the Andes are halved, dry air (<6 g kg^{-1}) is concentrated over and to the west of the SDC (Figs. 11c,d). Vertical cross sections of specific humidity taken south of Córdoba also show the environment between the Andes and SDC from the surface to near 4 km is 8–10 g kg^{-1} drier when the Andes are reduced relative to when the Andes are kept at full height (not shown). At 850 hPa, the greatest moisture in the lower-Andes runs is not directly downstream of the foothills but is farther north and east relative to the full Andes runs (Figs. 11c,d). Winds throughout the domain have a more westerly component, especially in the drier air over the SDC, and are about 5 m s^{-1} weaker north of the SDC. Once again, there are much smaller differences between the lAndes and lAndes_noSDC runs relative to the full Andes and reduced Andes runs suggesting the Andes play a larger role in the convective development relative to the SDC. In the noTer run, winds are completely from the west across the entire domain and drier air has advanced even farther east to 63°–64°W (Fig. 11e).

Results from this analysis highlight the relative importance of the Andes and SDC on the SALLJ. The greatest differences in low-level meridional winds and moisture are seen when the Andes are reduced or removed in comparison with when the SDC are removed. In the full-Andes cases, two maxima in northerly winds are identified over the plains that coincide with convective development. The largest moisture anomaly occurs along the SDC longitude toward the beginning of the second northerly wind maximum. In the half-Andes cases, only one wind maximum is identified in the morning hours over the plains. The winds are 5 m s^{-1} weaker across the domain and dry air surges in from the west several hours earlier relative to the full-Andes cases, which prevents convection from developing over the foothills in the afternoon and evening. When the Andes are completely removed there is no low-level jet signature and dry air restricts convective development to the eastern portion of the domain. These results suggest the unique height of the Andes is essential in the maintenance of the SALLJ and MCS development under strong synoptic conditions.

d. *MCS evolution*

The detailed convective characteristics of the MCSs for each experiment will be analyzed in future work. However, a summary of the MCS development in each of the simulations is shown in Fig. 12. At 2100 UTC 13 December, convection is beginning to develop over the southern SDC in the CTRL run and over the Andean foothills (Fig. 12a). Additionally, there is a larger system that persisted the entire day over Uruguay and the eastern edge of Argentina near Buenos Aires, Argentina. At this time, the lee cyclone has reached its lowest pressure (Fig. 7a). About 2–3 h earlier, 850-hPa moisture is maximized over the SDC (Fig. 10a) and northerly winds are beginning to increase farther east (Fig. 9a). In the noSDC run, convection initiation occurs over the Andes at about the same time, and the large system to the east is also present (Fig. 12b). Six hours later, convection has grown upscale into a large linear feature that is oriented northwest to southeast and extends from about 66°W to the Atlantic Ocean in both the CTRL and noSDC runs (Figs. 12f,g). The MCS slowly moves to the northeast, and by 0600 UTC is still a strong linear system that has just passed over Córdoba (Figs. 12k,l). Interestingly, more rain falls across the RELAMPAGO domain relative to the CTRL when the SDC are removed (noSDC rain accumulation is 104.6% of CTRL; Table 2). Given the environmental similarities between the two simulations and

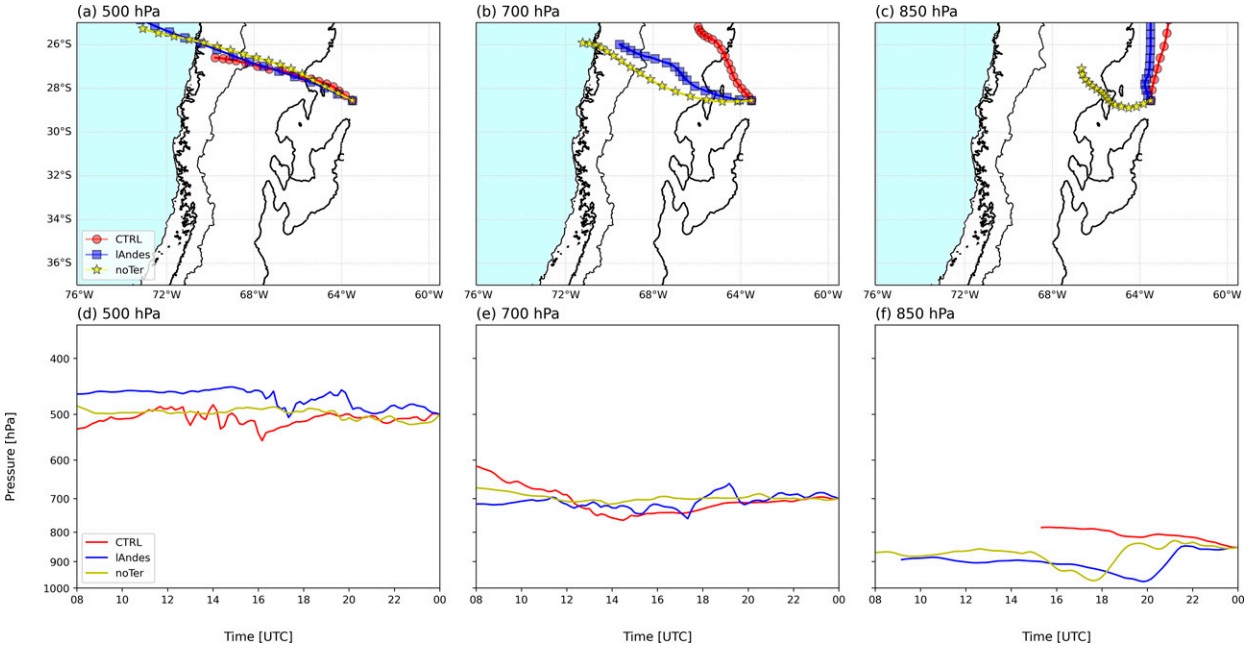

FIG. 8. Back-trajectories calculated from 0000 UTC 14 Dec every 10 min using RIP: (a)–(c) parcel locations and (d)–(f) time series of parcel pressures (hPa) at (left) 500, (middle) 700, and (right) 850 hPa for the CTRL (red), lAndes (blue), and noTer (yellow) simulations. Symbols in (a)–(c) represent each hour, the 500-m terrain contour is shown in black, and the "C" represents Córdoba.

the strength of the synoptic flow, it is not surprising that both full-Andes cases produce a strong MCS.

When comparing the full-Andes runs with the half-Andes runs, some significant differences stand out. Weaker convection initiates over the southern SDC around 1600 UTC in the lAndes case and there is no development off the Andean foothills like in the CTRL. The primary forcing for convection in the half-Andes runs is the cold front rather than topography. At 2100 UTC, both lAndes and lAndes_noSDC cases have a smaller linear system already well into the domain (Figs. 12c,d). There are no isolated features over the Andes at this time like there are in the full-Andes simulations (Figs. 12a,b). At 0300 UTC, the line has already passed Córdoba in both half-Andes runs (Figs. 12h,i). The lAndes MCS is narrower and does not extend as far east as the CTRL and noSDC MCSs. The lAndes_noSDC MCS is not nearly as intense as either the lAndes or full-Andes MCSs at this time. However, three hours later there seems to be some reinvigoration, and the convective lines between the lower-Andes cases are more similar (Figs. 12m,n). Accumulated rain across the RELAMPAGO domain in the lAndes run is about 56% of the CTRL run, while it is 67% of the CTRL in the lAndes_noSDC run (Table 2). When the Andes are reduced by 50%, rainfall is also reduced by nearly 50%. Similar to the full-Andes cases, when the SDC are removed, accumulated rain increases. The noTer simulation does not end up producing an MCS in the overnight hours, and there is weaker isolated convection scattered across the eastern portion of the domain (Figs. 12e,j,o). Accumulated rainfall is about 46% of the CTRL, which corresponds well with the drier air observed in Figs. 10e and 11e.

In all of the terrain-modification experiments, an MCS develops as a result of the passage of a cold front associated with strong synoptic forcing. However, the timing, location, and intensity of the MCS differs significantly between runs. In the full-Andes runs, the MCS reaches peak intensity around 0300 UTC 14 December (midnight local time). When the Andes are reduced by 50%, the resulting MCSs move faster to the east and are smaller and weaker than the full-Andes MCSs. Additionally, the accumulated rainfall is greater when the SDC are removed. One hypothesis for this is the SDC may interfere with the cold front structure and progression under strong synoptic forcing. Plots of equivalent potential temperature show a more cohesive cold front when the SDC are removed (not shown) supporting this hypothesis, but these perspectives will be explored in future work.

4. 25–26 January 2019: Weakly forced case

a. Overview

To understand more carefully the interactions between the synoptic flow and terrain in SSA, a second set of terrain-modification simulations was conducted on the 25–26 January 2019 case. This was another intense upscale growth case that featured convective echo tops greater than 20 km in height and had the greatest number of lightning flashes captured by the lightning mapping array network during RELAMPAGO (Schumacher et al. 2021; Nesbitt et al. 2021; Lang et al. 2020). This case was chosen because it was not strongly synoptically forced like the December case. A short-wave trough passed over the southern Andes at around 45°S

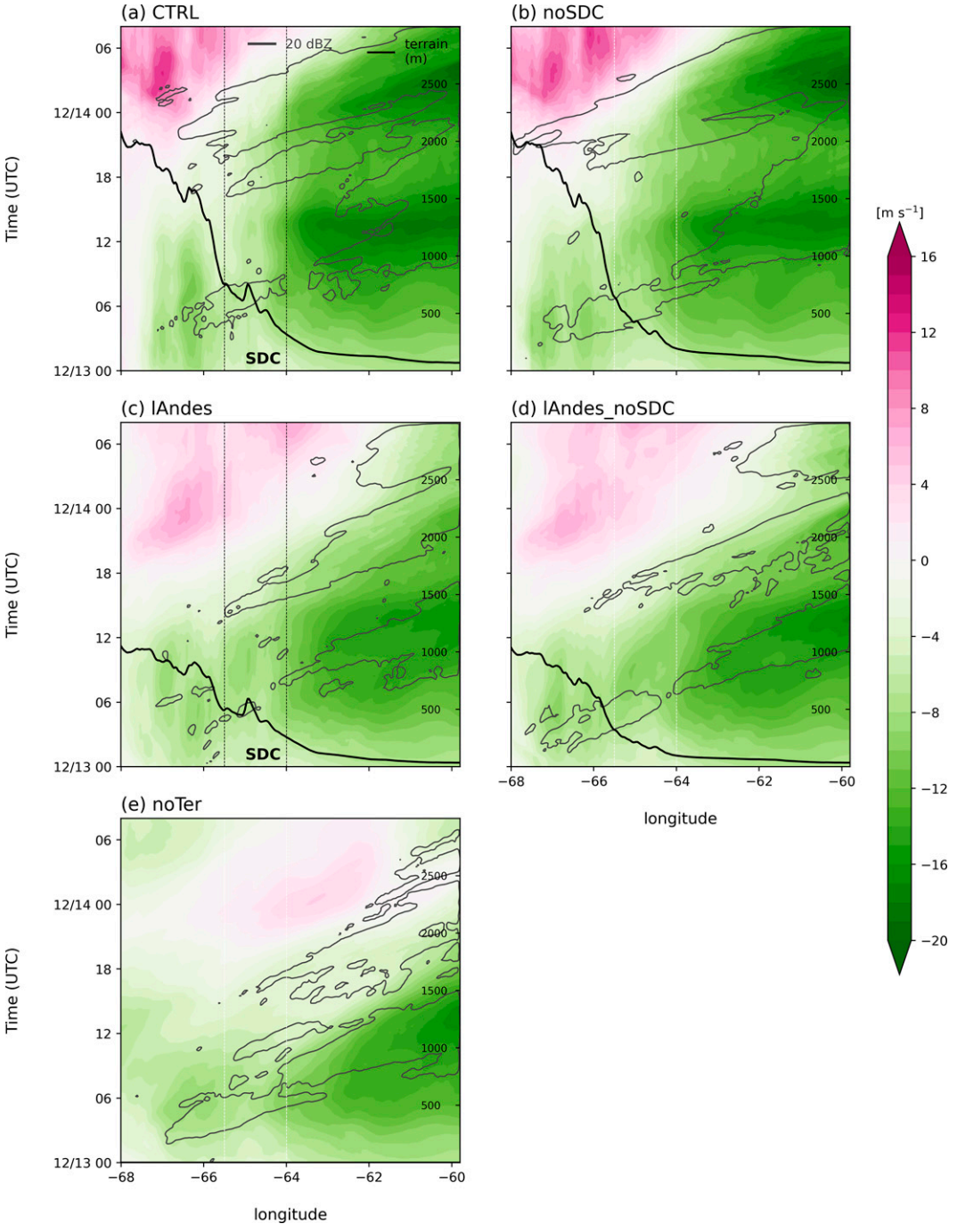

FIG. 9. Hovmöller diagrams of 850-hPa meridional winds (shaded; m s^{-1}) from the 3-km domain averaged across the SALLJ domain and 20-dBZ composite reflectivity (gray contour; dBZ) from the 3-km domain averaged across the RELAMPAGO domain for the (a) CTRL, (b) noSDC, (c) lAndes, (d) lAndes_noSDC, and (e) noTer simulations. Longitude ranges from about 68° to 60°W, and times are shown from 0000 UTC 13 to 0800 UTC 14 Dec. The average terrain profile from the 3-km domain averaged across the SALLJ domain is shown with the black contour. The location of the SDC is shown within the dashed black lines in (a) and (c), and where the SDC would be is shown within the dashed white lines in (b), (d), and (e).

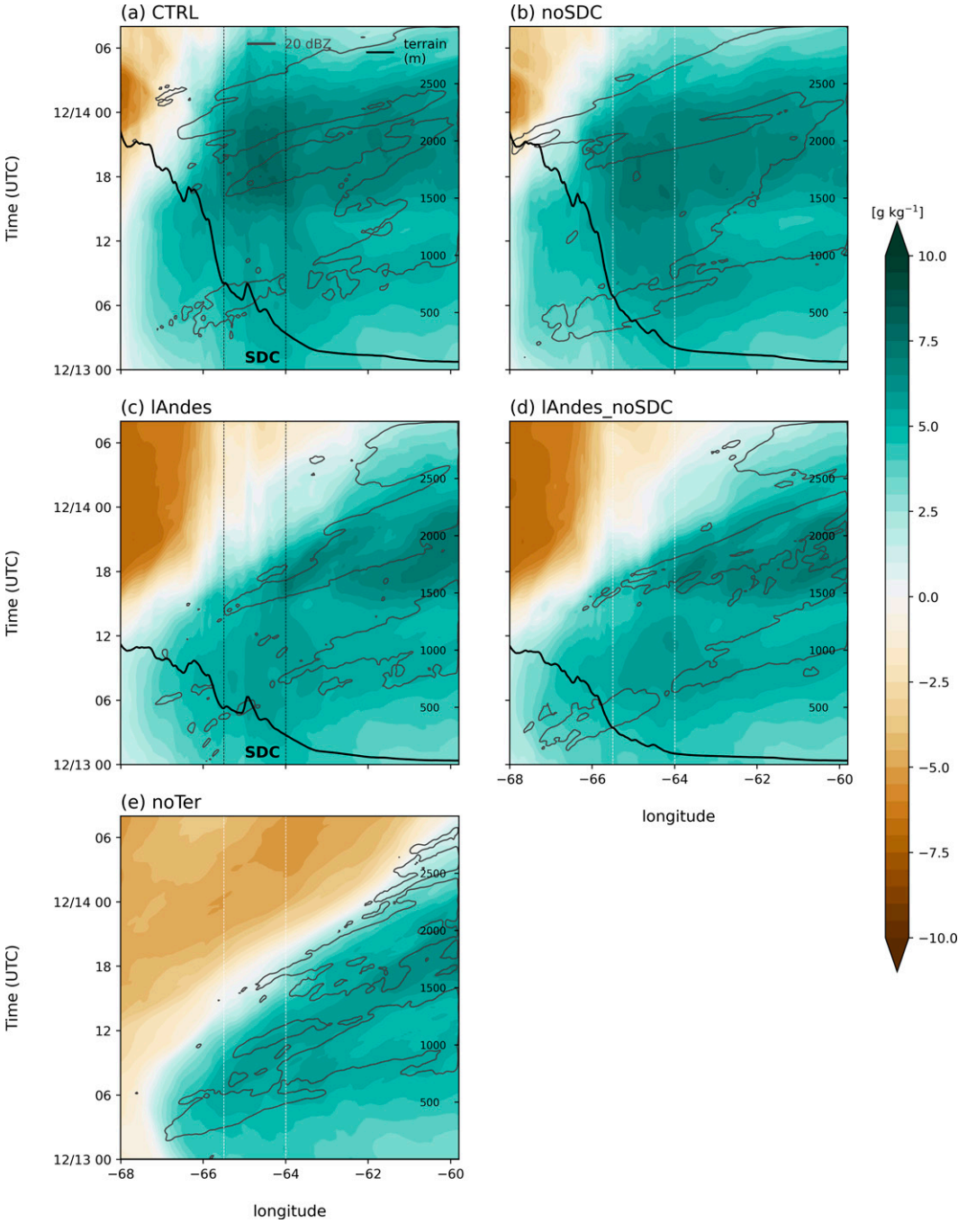

FIG. 10. As in Fig. 9, but for 850-hPa specific humidity anomalies (shaded; g kg^{-1}), calculated from monthly mean ERA5 reanalysis data from 1978 to 2018.

while the flow over Córdoba was weakly zonal at 500 hPa (Fig. 13a). There was a significant amount of moisture within the region that was funneled south by the SALLJ and maximized at 18 g kg^{-1} over the SDC (Fig. 13b). Specific humidity values greater than 10 g kg^{-1} were seen as far south as 48°S and appeared to wrap around the high pressure over the Atlantic. Unlike the strongly forced case, the MCS that formed remained tied to the SDC for an extended period of time, and the WRF CTRL simulation did a reasonable job of capturing the intense convection and life cycle of upscale growth in the region (Figs. 13c,d).

b. *Synoptic scale and SALLJ*

Hovmöller plots of 500- and 850-hPa heights clearly show that the synoptic activity was much weaker relative to the strongly forced case (Fig. 14). The minimum average 500-hPa

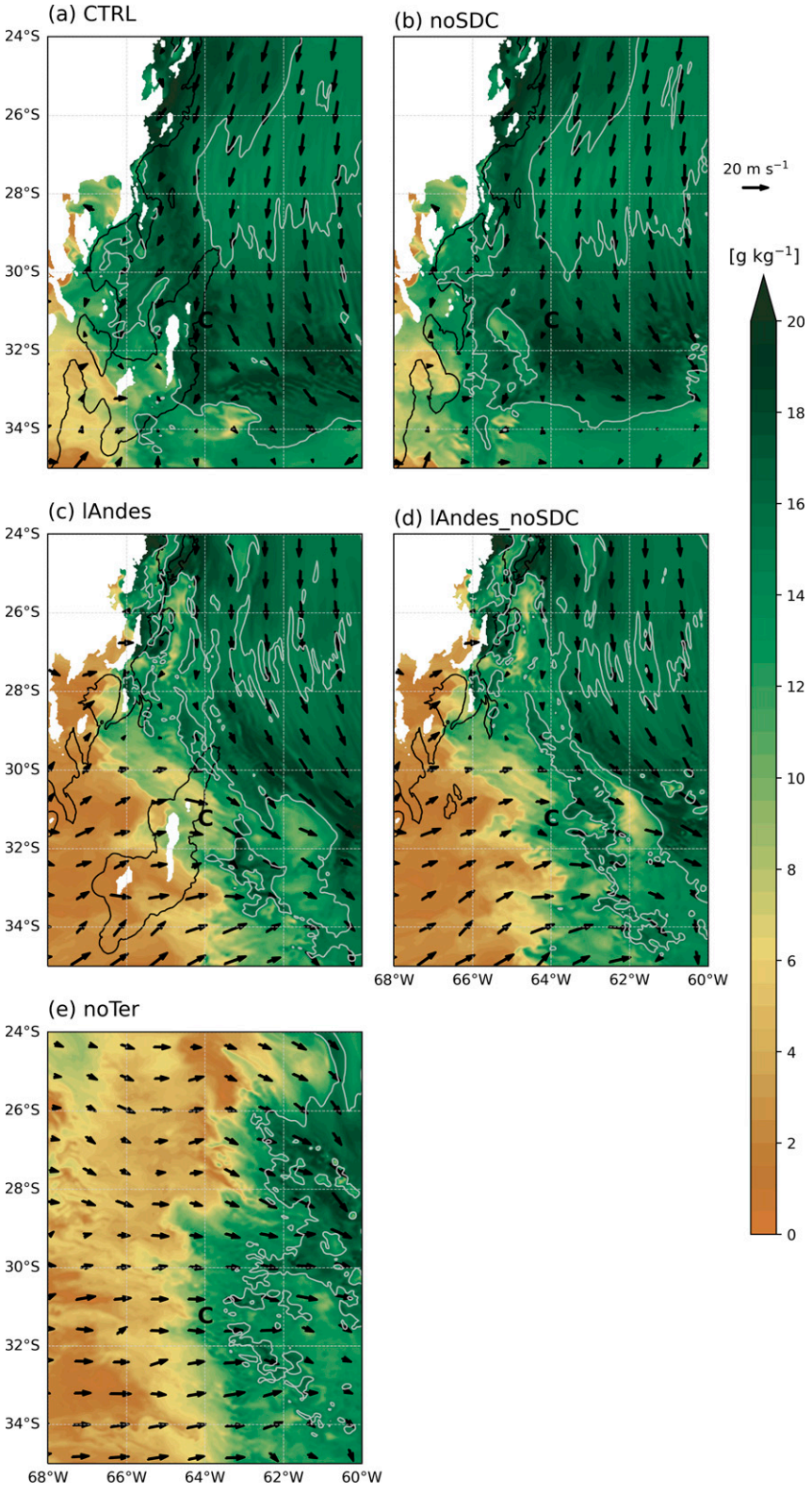

FIG. 11. The 850-hPa specific humidity (shaded; g kg^{-1}) and winds (arrows; m s^{-1}) from the 3-km domain at 2100 UTC 13 Dec 2018, shown across the SALLJ domain, for (a) CTRL, (b) noSDC, (c) lAndes, (d) lAndes_noSDC, and (e) noTer simulations. The 15 g kg^{-1} contour is shown in gray. The 500-m terrain contour is shown in black, and the "C" represents Córdoba.

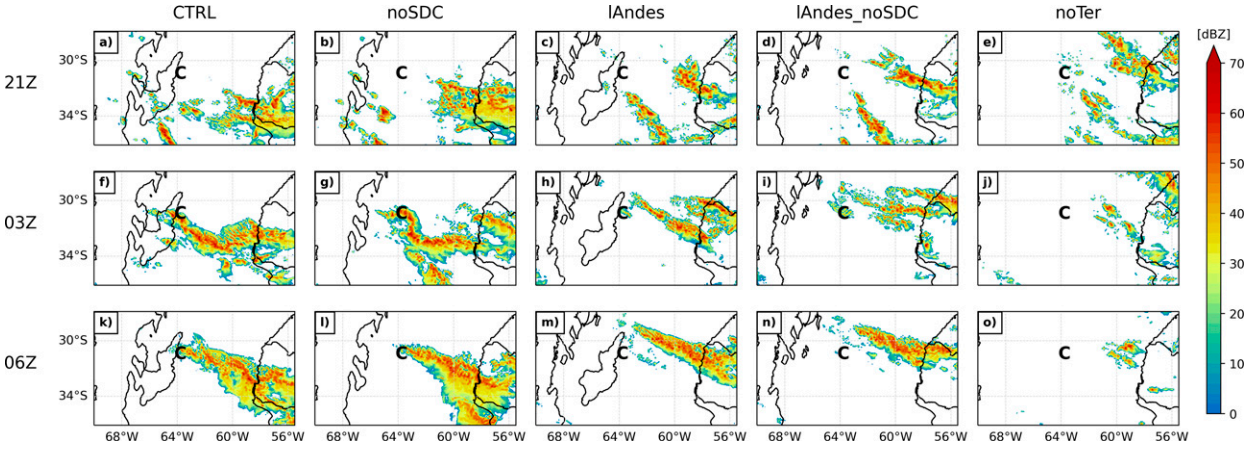

FIG. 12. Reflectivity at 3 km MSL for each simulation (columns) at (a)–(e) 2100 UTC 13 and (f)–(j) 0300 and (k)–(o) 0600 UTC 14 Dec. The 500-m terrain contour is shown in black, and the "C" represents Córdoba.

geopotential height of 5672 m is achieved just west of the Andes between 0600 and 1200 UTC 25 January (Fig. 14a). This is about 100 m higher than the trough on 13 December. Interestingly, when the Andes are reduced and removed, the 500-hPa short wave does not strengthen like in December (Figs. 14b,c). At 850 hPa, lee cyclogenesis is visible in the CTRL run between 1800 and 0000 UTC over the higher terrain of the Andes, but again this is not as strong as the strongly forced case and the minimum geopotential height achieved is 1452 m (about 60 m higher than the December lee cyclone). Convection also starts to develop when the lee cyclone is maximized. Unlike the strongly forced case, there is a secondary peak in convection that is tied to the terrain between the Andes and SDC. This back-building component is not as visible when the Andes are lowered and is not present at all when the terrain is removed. Similar to the strongly forced case, geopotential heights in the lAndes and noTer simulations are higher than the CTRL, highlighting the influence of the terrain on the development of the lee cyclone in a weak synoptic forcing case.

The strength of the 850-hPa jet is also analyzed across terrain-modification runs for the weakly forced case. There is a single maximum in northerly winds located just east of 64°W, downstream of the SDC (Fig. 15). The strongest northerly flow occurs between 0000 and 1500 UTC 25 January, where winds reach a maximum magnitude of 18–20 m s^{-1} (on average) at 0900 UTC for all runs. This area of enhanced northerlies (>10 m s^{-1} magnitude) extends farther east and west when the SDC are removed and when the Andes are removed (Figs. 15b,d,e). This timing agrees with Sasaki et al. (2022) who show that shorter-duration jets are driven more by boundary layer processes and the diurnal cycle. Weak southerly flow is observed in the CTRL and noSDC runs over the higher terrain starting around 0000 UTC 26 January (Figs. 15a,b). This flow is about 5 m s^{-1} weaker than the southerly flow in the strongly forced case. There are few differences between the CTRL and noSDC wind patterns near the higher terrain. Interestingly, the back-building convection visible in the CTRL run develops in southerly flow and this back-building component is not visible when the SDC are removed.

Moisture anomalies are also calculated for this case using the January monthly means from ERA5. The average 850-hPa specific humidity across the domain during January is 9.7 g kg^{-1}, about 1 g kg^{-1} moister than December. Hovmöller plots of 850-hPa specific moisture anomalies show increased moisture over the higher terrain early in the period from 0000 to 1800 UTC 25 January (Fig. 16). These values are maximized in the CTRL and noSDC cases at 7.5 and 7.7 g kg^{-1}, respectively (Figs. 16a,b). They are about 0.5 g kg^{-1} weaker when the Andes are halved, but the moisture patterns are similar between the full-Andes and half-Andes runs (Figs. 16c,d), unlike in the strongly forced case (Fig. 10). Vertical cross sections of specific humidity averaged south of Córdoba at 2100 UTC 25 January show moisture is present as high as 8 km above ground, which is about 3 km deeper than moisture available in December (not shown). The region between the Andes and SDC in the CTRL simulation has equivalent potential temperature values about 10 K warmer than the strongly forced CTRL. Additionally, specific humidity values greater than 20 g kg^{-1} extend more than 500 km downstream of the SDC at the surface in the weakly forced

TABLE 2. Accumulated rainfall (mm) from the 3-km domain summed across the RELAMPAGO domain from 1500 UTC 13 Dec to 0800 UTC 14 Dec (first row) and from 1500 UTC 25 Jan to 1800 UTC 26 Jan (second row). The percentage of the CTRL is shown in parentheses.

Run	CTRL	noSDC	lAndes	lAndes_noSDC	noTer
Dec	855 029	8 904 666 (104.6%)	476 990 (55.8%)	573 149 (67.0%)	394 887 (46.2%)
Jan	1 864 352	1 384 152 (74.2%)	172 1603 (92.3%)	1 183 450 (63.5%)	856 166 (45.9%)

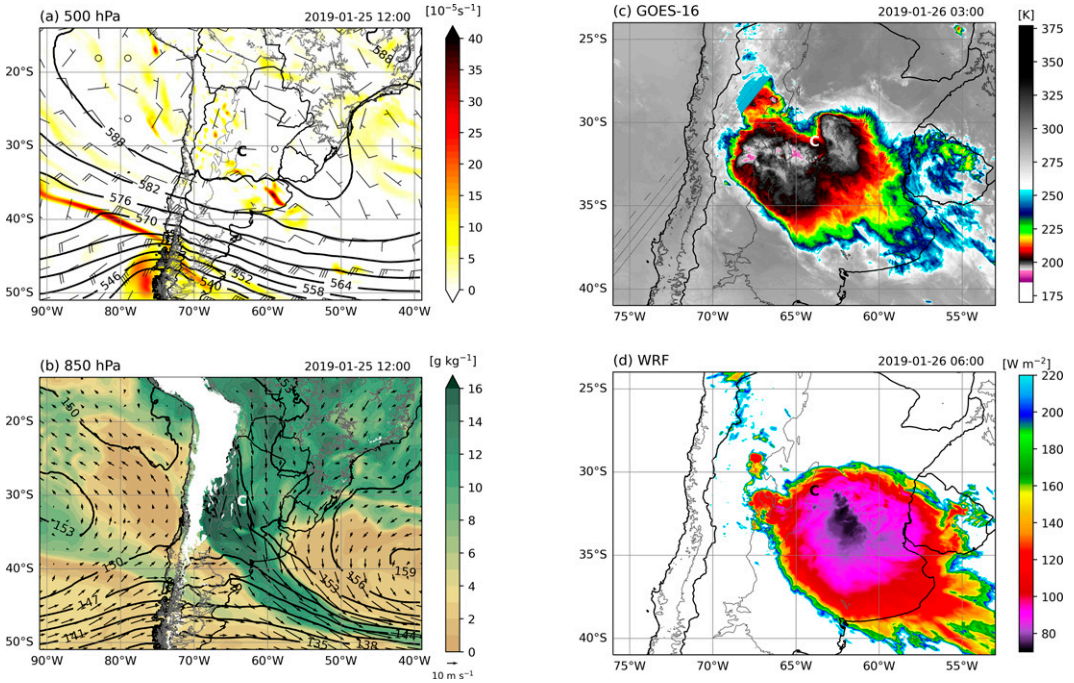

FIG. 13. (a) The 500-hPa geopotential heights (contoured; dam), relative vorticity (shaded; 10^{-5} s^{-1}), and winds (barbs; m s^{-1}, where a half barb is 5 m s^{-1} and a full barb is 10 m s^{-1}) from ERA5 reanalysis at 1200 UTC 25 Jan 2019, (b) 850-hPa geopotential heights (contoured; dam), specific humidity (shaded; g kg^{-1}), and winds (arrows; m s^{-1}) from ERA5 reanalysis at 1200 UTC 25 Jan 2019, (c) *GOES-16* channel-14 IR brightness temperatures (K) at 0300 UTC 26 Jan 2019, and (d) outgoing longwave radiation (W m^{-2}) from the 3-km CTRL simulation at 0600 UTC 26 Jan 2019. The 500-m terrain contour is shown in gray, and the "C" represents Córdoba.

runs, while the moisture maximum is only 100 km wide in the strongly forced runs and is not directly connected to the SDC.

Convection generally starts to develop at the end of the high-moisture period to the west of the SDC in each simulation around 1800 UTC 25 January. Moisture is only 1–2 g kg^{-1} higher than normal over the eastern plains across all the simulations, possibly explaining why the convection was more focused on the terrain in this case than in the strongly forced case with more widespread moisture anomalies east of the SDC. The atmosphere tends to dry out during and after the convection, especially right downstream of the SDC in the CTRL and lAndes runs (Figs. 16a,c). In fact, at 1200 UTC 26 January, moisture anomalies are 2–4 g kg^{-1} lower in the CTRL and lAndes runs relative to the noSDC and lAndes_noSDC runs at 64°W (Figs. 16a–d). When the Andes are removed, moisture anomalies are generally weaker to the east relative to when the Andes are present, and there is slightly drier air (~2 g kg^{-1} less than normal) present over the western domain (Fig. 16e). There is no convective development later in the period since there is no terrain to help to initiate convection.

Results from this weakly forced case analysis provide an important contrast to those from the strongly forced case. First, the upper-level flow was significantly weaker than in the strongly forced case, and 500- and 850-hPa heights increased when the Andes were reduced/removed. A lee cyclone still developed in the evening hours with the full-Andes, but it was not as deep as in the strongly forced case. The SALLJ was also present in this weakly forced case, but it was located farther west and a single maximum in northerly winds was identified in the morning hours, consistent with shorter-duration jets identified in Sasaki et al. (2022). The jet strength was weaker when the Andes were reduced, but the location and timing were similar to the full-Andes. The greatest moisture anomalies were concentrated to the west of the SDC in the full-Andes and half-Andes runs, and there was no intrusion of dry air like in the strongly forced case. The environments with full-Andes and half-Andes were much more similar than the strongly forced case, but the timing and location of convection was considerably different across runs.

c. *MCS evolution*

The life cycle of the storm is shown at three times in Fig. 17. At 2100 UTC 25 January, convection initiates over the Andes and the southern SDC in the CTRL run (Fig. 17a). Similar initiation over the Andes is seen in the noSDC case, but the secondary convection around 66°W is not visible (Fig. 17b). Six hours later, a large convective line develops in the CTRL run that stretches from the SDC to the Atlantic Ocean (Fig. 17f). In the noSDC run, the convective line remains tied to the Andean foothills but does not extend as far east as the Atlantic (Fig. 17g). At 1500 UTC 26 January, there is

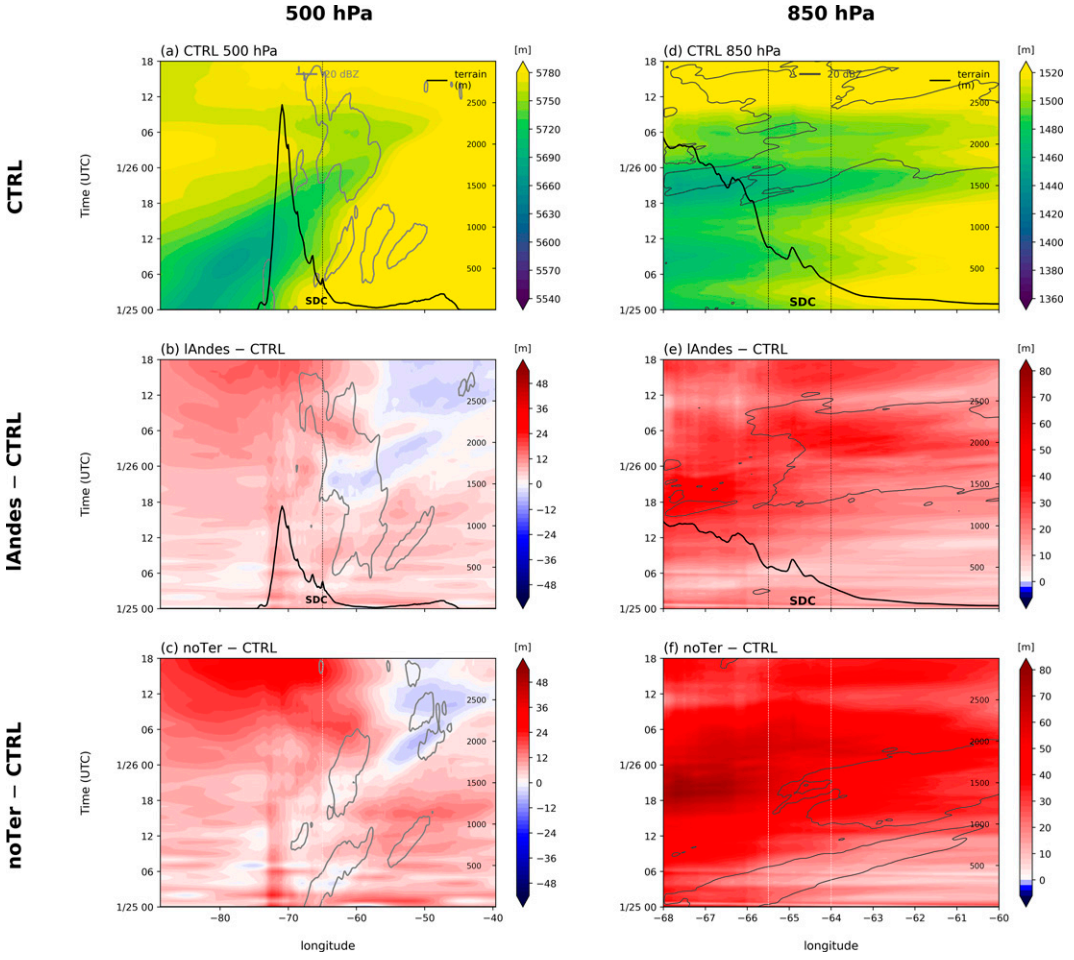

FIG. 14. (a)–(c) As in Fig. 5 and (d)–(f) as in Fig. 7, but for the weakly forced case. Longitude ranges from about 90° to 40°W for (a)–(c) and from about 68° to 60°W for (d)–(f), and times are shown from 0000 UTC 25 to 1800 UTC 26 Jan.

significant precipitation northwest of Córdoba between the foothills and the SDC in the CTRL run (Fig. 17k). At 3 km MSL, the intensity is generally less than 40 dBZ. This back-building and the direct connection to the SDC are removed when the SDC are removed, and weaker convection is visible across the eastern plains (Fig. 17l). The accumulated rainfall across the RELAMPAGO domain is less in the noSDC run than in the CTRL (74% of CTRL; Table 2), with the largest differences occurring between 0000 and 0600 UTC 26 January (not shown).

When the Andes are reduced by 50%, a convective line still forms when the SDC are present (Fig. 17c). This line is within the domain at 2100 UTC, suggesting that convective initiation begins earlier when the Andes are reduced and moves eastward faster. At 0300 UTC, the line is positioned just south of Córdoba but is oriented more zonally in comparison with the MCS in the CTRL run (Fig. 17h). At 1500 UTC, weak back-building in the northwest portion of the domain is visible, although not as intense as in the CTRL run (Fig. 17m). This signature is also visible in the Hovmöller plots, and the total rainfall summed across the RELAMPAGO domain for the lAndes case is second highest (92% of the CTRL; Table 2). When the Andes are reduced and SDC are removed, a convective line does not develop (Figs. 17d,i,n). Isolated convection downstream of the Andes is visible at 2100 UTC (Fig. 17d), and a weaker, unorganized system is present at 0300 UTC (Fig. 17i). Only isolated convection remains at 1500 UTC (Fig. 17n), and the accumulated rainfall is 63.5% of the CTRL. These results are similar for when the terrain is completely removed (Figs. 17e,j,o). A smaller system still develops but is likely driven by the diurnal sea-breeze and a weaker baroclinic trough.

Similar to the strongly forced case, convection develops in each terrain-modification experiment, but the location, timing, and intensity of the convection vary significantly. A robust MCS develops in the CTRL and lAndes simulations that produces similar amounts of rainfall. There is a strong sign of back-building in these runs. When the SDC are removed, the rain accumulation is reduced by nearly 25%

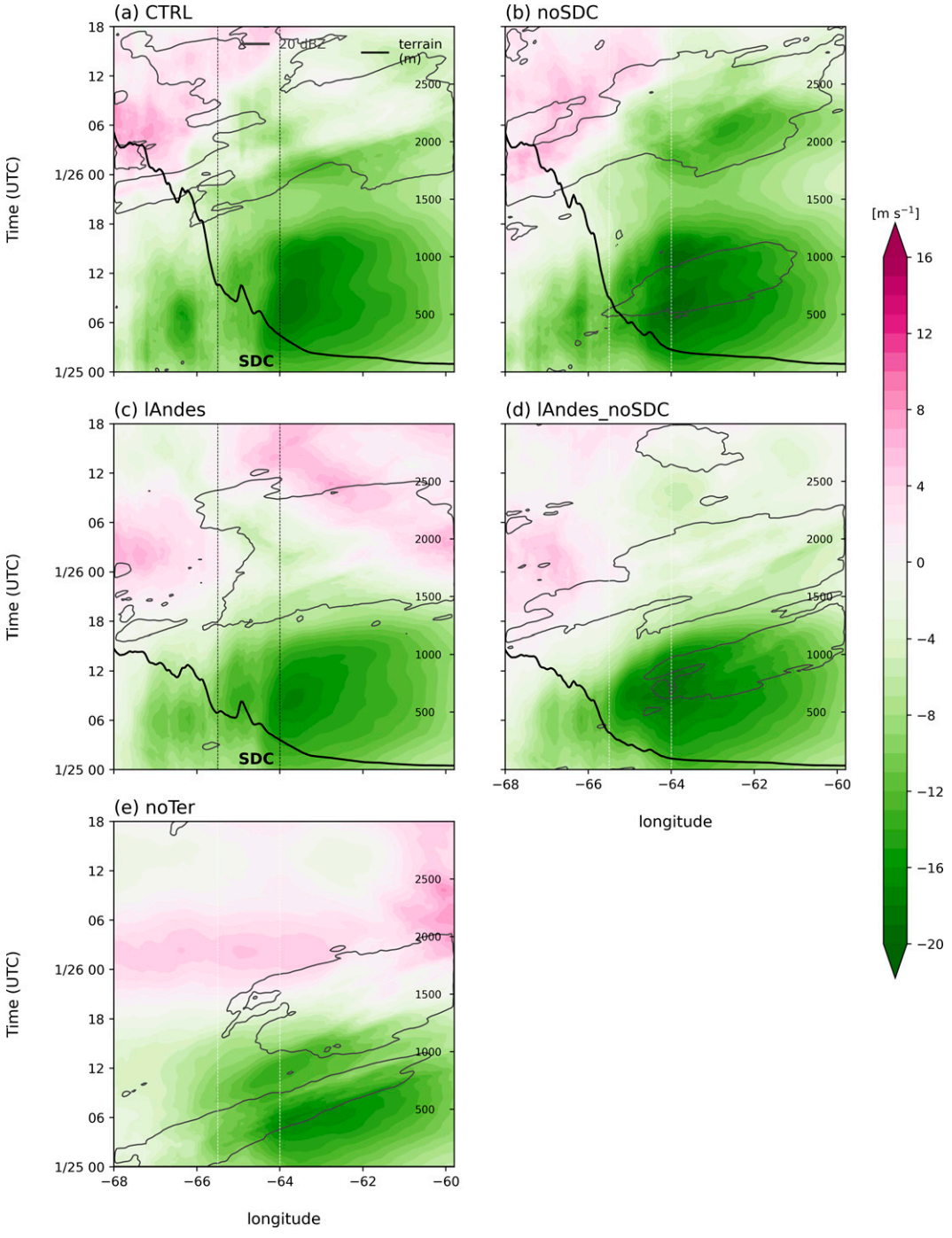

FIG. 15. As in Fig. 9, but for the weakly forced case. Times are shown from 0000 UTC 25 to 1800 UTC 26 Jan.

and there is no strong connection to the topography. These results contrast with those from the strongly forced case where the height of the Andes appeared to play a more important role in the MCS evolution relative to the SDC. The environments under the weakly forced case for the full-Andes and half-Andes runs were similar, despite producing different MCSs, suggesting the SDC may be more important in convective development under weak synoptic conditions.

5. Discussion

Two RELAMPAGO cases in December 2018 and January 2019 were chosen since they both produced a large MCS that

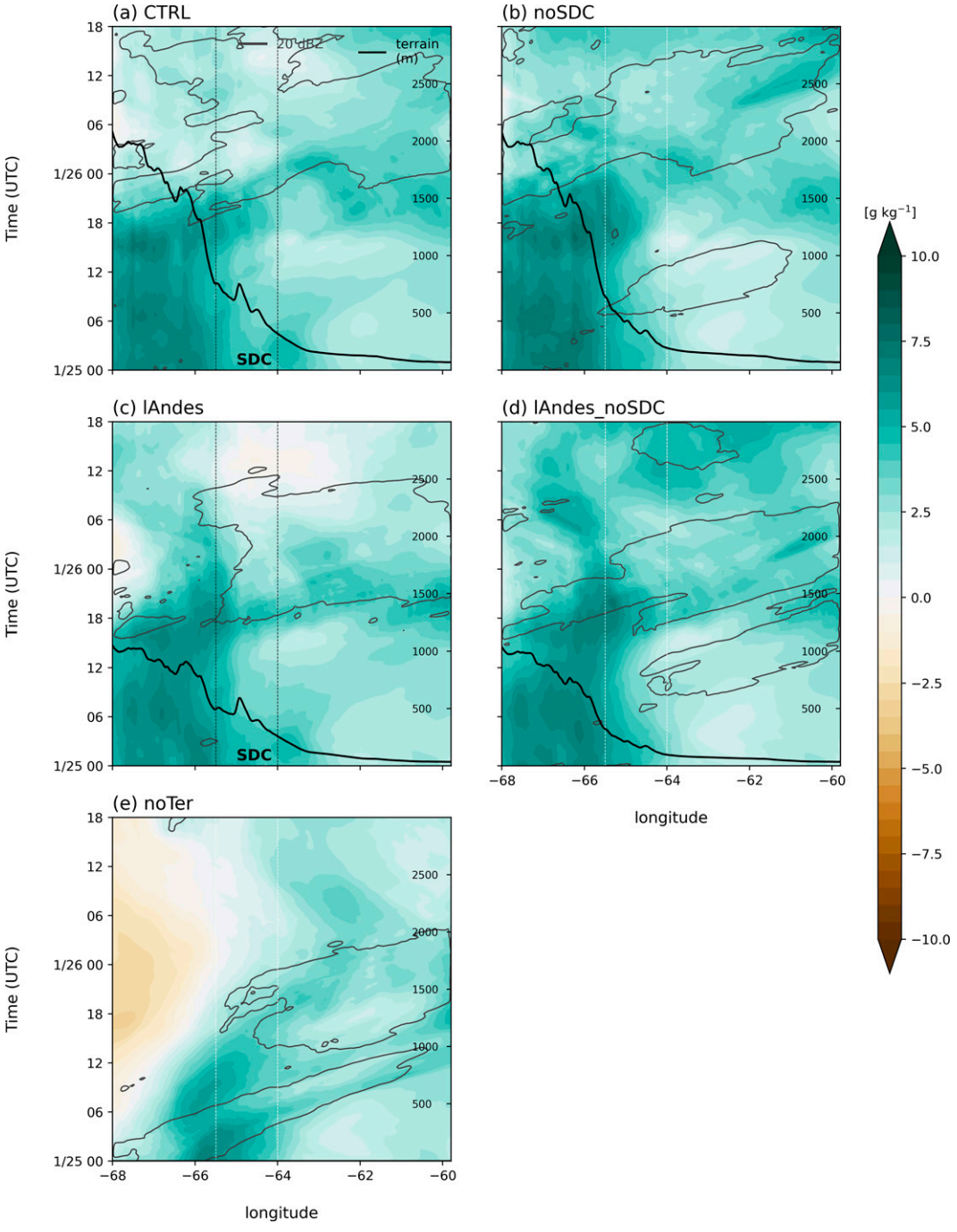

FIG. 16. As in Fig. 10, but for the weakly forced case. Times are shown from 0000 UTC 25 to 1800 UTC 26 Jan.

resulted in severe weather, flooding, and extreme lightning flash rates, but the synoptic forcing supporting convective development and upscale growth was significantly different between the two. A strong synoptic trough passed over the Andes during the December case, which led to the development of a robust lee cyclone in the Córdoba region. During the January case, however, a weak short wave passed through the midlatitudes with zonal flow over the Córdoba region that resulted in a weaker lee cyclone. In the simulations, when the Andes are reduced by 50% for the strongly forced case, the upper-level trough is able to cross the southern Andes without being sheared apart. A lee cyclone also develops downstream, but it is not as intense as when the Andes are at full height. The impact of reducing the Andes during the weakly forced case is a slightly weaker short-wave trough aloft and a weaker lee cyclone as well.

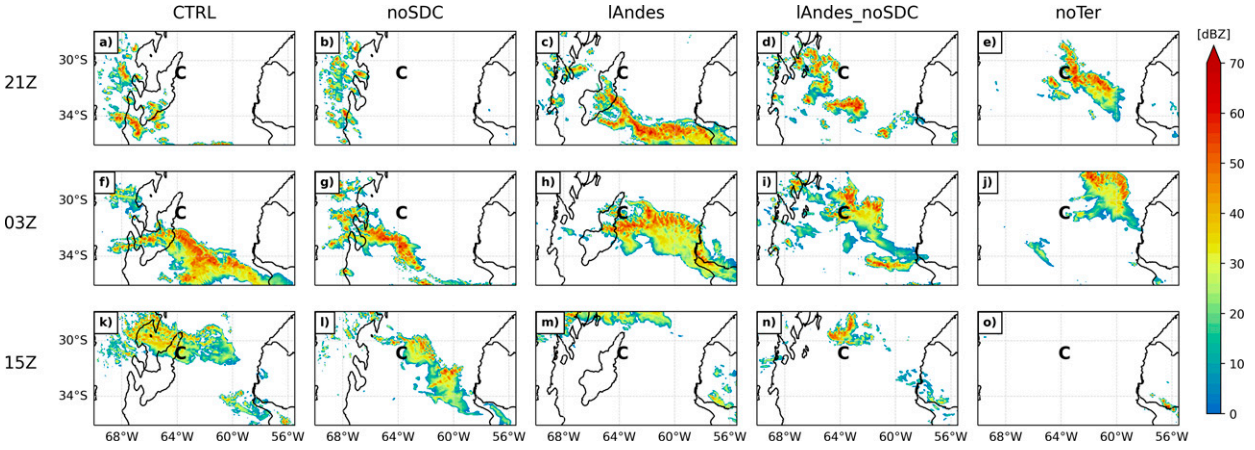

FIG. 17. As in Fig. 12, but for the weakly forced case. Times displayed are 2100 UTC 25 and 0300 and 1500 UTC 26 Jan.

In terms of the SALLJ, two northerly wind maxima at 850 hPa are observed in the CTRL and noSDC runs for the strongly forced case that occur over the eastern plains. When the Andes are reduced, these wind maxima are also reduced in magnitude. In the weakly forced case, however, a single northerly wind maximum is observed directly downstream of the SDC in all terrain-modification experiments in the overnight/morning hours. Meridional wind patterns are similar across experiments in the weakly forced case. Although the weakly forced case was not included in the sounding analysis by Sasaki et al. (2022), we hypothesize this event would fit into their "shorter duration jet" classification. To further explore the impact of terrain on the SALLJ under strong and weak synoptic environments, the meridional flow was averaged across the northern half of the SALLJ domain at different heights (Fig. 18). Under strong synoptic forcing, the jet in the full-Andes runs has a broad maximum of -10 m s^{-1} that stretches from ~900 to 775 hPa (Fig. 18a). When the Andes are halved though, the depth of the jet is smaller, reaching a maximum of about -7.5 m s^{-1} around 850–825 hPa. There is no clear jet signature in the noTer run, consistent with the Hovmöller plots and the ingredients necessary for a SALLJ

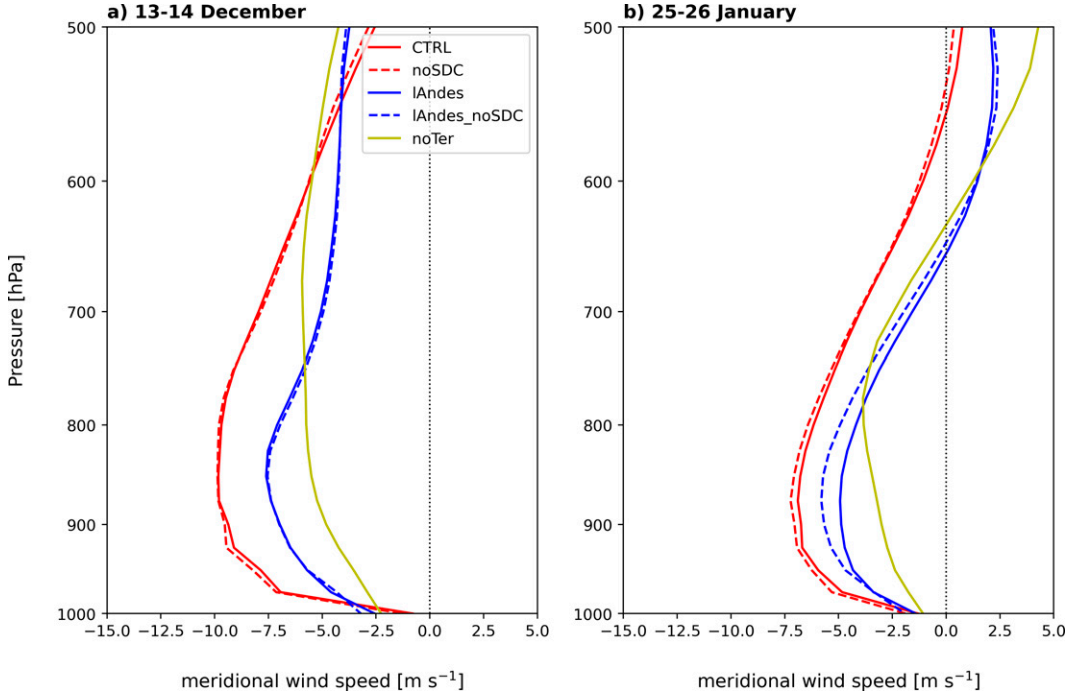

FIG. 18. Vertical profiles of meridional wind speed averaged across the northern SALLJ domain (north of 30°S) and across times (a) 0000 UTC 13–0800 UTC 14 Dec and (b) 0000 UTC 25–1800 UTC 26 Jan for the CTRL (red), lAndes (blue), and noTer (yellow) simulations.

(i.e., sloping terrain). These results agree well with Sasaki et al. (2022) who show that long-duration jets are often deeper and occur under stronger synoptic flow. The height of the Andes appears to control the depth of the jet, and this may explain why jets in the United States are often shallower, consistent with the lower height of the Rockies. Under weak synoptic forcing, the depth of the jet does not change between full-Andes and half-Andes runs (Fig. 18b). The maximum is achieved around 900–850 hPa and is 2–4 m s^{-1} weaker than in the strongly forced case. These jets are driven by boundary layer processes rather than the synoptic flow.

For the moisture associated with the SALLJ, higher values of specific humidity are observed at 850 hPa during the weakly forced case than during the strongly forced case. However, taking climatology into context, the strongly forced case has higher anomalous moisture values than does the weakly forced case. In addition to differences in moisture, the locations of the moisture maxima are different between the two cases. In December, the moisture maximum is concentrated downstream of the SDC, whereas it is farther west over the higher terrain of the Andes during January. This agrees with Rasmussen et al. (2014) who showed a shift in moisture and convection to the west during the summer months. When the Andes are reduced during the strongly forced case, anomalously dry air is concentrated over the mountains later in the period, which prevents convection from developing over the terrain. However, during the weakly forced case when the Andes are reduced, the moisture patterns are very similar to when the Andes are at full height.

The broad convective patterns analyzed are also different between the two cases. In the strongly forced case, a large MCS develops in each terrain-modification experiment simply due to the strong synoptic forcing and low-level convergence associated with the robust lee cyclone interacting with the northerly SALLJ (RH16; Piersante et al. 2021). The position and intensity of the MCS are similar between the CTRL and noSDC runs suggesting the SDC do not have a large impact on the overall structure of the system. The accumulated rainfall is also highest in the CTRL and noSDC runs during December. When the SDC are removed, rainfall actually increases during the strongly forced case. In this case, the SDC may interfere with the passing cold front, which could reduce precipitation. In the weakly forced case, however, the most rain falls in the CTRL and lAndes runs. Both simulations have convection redevelop between the Andes and SDC, which does not occur when the SDC are removed. This once again highlights the importance of the SDC in forcing convection under weak synoptic conditions. In both December and January cases, convection tends to move off the terrain faster when the Andes are reduced. Additionally, when the terrain is removed, a single system develops, moves toward the east, and dissipates, as one might expect an idealized MCS to do. These results all suggest that under strong synoptic conditions, the height of the Andes plays a larger role in modulating the environment and the evolution of the MCS relative to under weaker synoptic conditions when the SDC act to enhance convective development and keep the MCS tied to the terrain.

6. Conclusions

Two RELAMPAGO cases of upscale growth are studied using terrain-modification WRF simulations to investigate how the convective development and synoptic-scale environmental conditions varied in strongly and weakly forced synoptic environments. Five experiments were run on the 13–14 December 2018 case, which exhibited a deep upper-level trough and strong lee cyclogenesis, and another five simulations were run on the 25–26 January 2019 case, which exhibited a weak shortwave trough that passed over the Andes in the midlatitudes. Each case study had a CTRL simulation in which the terrain was not modified, a noSDC run in which the SDC were removed, a lAndes run in which the Andes were reduced by 50% and SDC were kept at the same height, a lAndes_noSDC run where the Andes were halved and SDC were removed, and a noTer run in which terrain was reduced to 0 m across the domains. Analyses of the terrain-modification simulations for both cases led to the following general conclusions:

1) Under strong synoptic flow, the height of the Andes, rather than the SDC, has a greater impact on the environment and convective growth associated with MCSs. A large MCS develops in all scenarios simply because of synoptic forcing, but the environment and SALLJ are significantly altered when the Andes are reduced.
2) Under weak synoptic flow, the SDC have a more direct impact in forcing convection and the environment is more similar for different terrain-modification runs. Mesoscale and orographic processes are likely more important in forcing convection in these cases, including diurnal heating and mountain flow patterns.
3) The Andes are a unique height that allows systems to rapidly grow upscale while remaining tied to the terrain. The SDC are a secondary feature that aids in convection initiation and redevelopment, especially under weaker synoptic flow, which leads to prolonged convective events in the Córdoba region.

These results generally focused on large-scale changes to the environment and convection. Future work will use ground-based observations from RELAMPAGO and the Cloud, Aerosol, and Complex Terrain Interactions (CACTI) field campaign and 1-km grid spacing WRF simulations of the CTRL and select terrain-modification experiments to evaluate the frequency, intensity, and structure of convective features produced during the strongly and weakly forced cases. Specific focus will be on how the SDC alter the intensity and location of updrafts within the system, how the terrain impacts the development and propagation of cold pools, and the role of the SDC in producing high lightning flash counts in the Córdoba region. This study, in conjunction with future work, provides a better insight into what drives intense convection in this region of the world.

Acknowledgments. This research was supported by NSF Grants AGS-1661657 and AGS-2146709, DOE Grant DE-SC0022056, and a NASA FINESST Fellowship (NASA Grant

80NSSC21K1618). We thank Angela Rowe, Lynn McMurdie, Clayton Sasaki, and Daniel Veloso Águila for their helpful comments and discussions. We also thank the three anonymous reviewers for their comments.

Data availability statement. WRF terrain-modification simulations are stored on a Colorado State University server. *GOES-16* imagery is accessible through the RELAMPAGO field catalog (https://data.eol.ucar.edu/master_lists/generated/relampago/). ERA5 data were accessed through Copernicus (https://cds.climate.copernicus.eu/cdsapp#!/home).

REFERENCES

Blackadar, A. K., 1957: Boundary layer wind maxima and their significance for the growth of nocturnal inversions. *Bull. Amer. Meteor. Soc.*, **38**, 283–290, https://doi.org/10.1175/1520-0477-38.5.283.

Bruick, Z. S., K. L. Rasmussen, and D. J. Cecil, 2019: Subtropical South American hailstorm characteristics and environments. *Mon. Wea. Rev.*, **147**, 4289–4304, https://doi.org/10.1175/MWR-D-19-0011.1.

Chen, F., and J. Dudhia, 2001: Coupling an advanced land-surface/hydrology model with the Penn State/NCAR MM5 modeling system. Part I: Model description and implementation. *Mon. Wea. Rev.*, **129**, 569–585, https://doi.org/10.1175/1520-0493(2001)129<0569:CAALSH>2.0.CO;2.

Copernicus Climate Change Service, 2017: ERA5: Fifth generation of ECMWF atmospheric reanalyses of the global climate. Copernicus climate change service climate data store, accessed 26 July 2021, https://cds.climate.copernicus.eu/cdsapp#!/home.

Dirmeyer, P. A., K. L. Brubaker, and T. DelSole, 2009: Import and export of atmospheric water vapor between nations. *J. Hydrol.*, **365**, 11–22, https://doi.org/10.1016/j.jhydrol.2008.11.016.

Du, Y., and R. Rotunno, 2014: A simple analytical model of the nocturnal low-level jet over the Great Plains of the United States. *J. Atmos. Sci.*, **71**, 3674–3683, https://doi.org/10.1175/JAS-D-14-0060.1.

Dudhia, J., 1989: Numerical study of convection observed during the Winter Monsoon Experiment using a mesoscale two- dimensional model. *J. Atmos. Sci.*, **46**, 3077–3107, https://doi.org/10.1175/1520-0469(1989)046<3077:NSOCOD>2.0.CO;2.

Holton, J. R., 1967: The diurnal boundary layer wind oscillation above sloping terrain. *Tellus*, **19**, 199–205, https://doi.org/10.1111/j.2153-3490.1967.tb01473.x.

Hong, S.-Y., Y. Noh, and J. Dudhia, 2006: A new vertical diffusion package with an explicit treatment of entrainment processes. *Mon. Wea. Rev.*, **134**, 2318–2341, https://doi.org/10.1175/MWR3199.1.

Houze, R. A., Jr., 2004: Mesoscale convective systems. *Rev. Geophys.*, **42**, RG4003, https://doi.org/10.1029/2004RG000150.

——, K. L. Rasmussen, M. D. Zuluaga, and S. R. Brodzik, 2015: The variable nature of convection in the tropics and subtropics: A legacy of 16 years of the Tropical Rainfall Measuring Mission satellite. *Rev. Geophys.*, **53**, 994–1021, https://doi.org/10.1002/2015RG000488.

Insel, N., C. J. Poulsen, and T. A. Ehlers, 2010: Influence of the Andes mountains on South American moisture transport, convection, and precipitation. *Climate Dyn.*, **35**, 1477–1492, https://doi.org/10.1007/s00382-009-0637-1.

Kain, J. S., and J. M. Fritsch, 1993: Convective parameterization for mesoscale models: The Kain-Fritsch scheme. *The Representation of Cumulus Convection in Numerical Models, Meteor. Monogr.*, No. 46, Amer. Meteor. Soc., 165–170.

Kummerow, C., W. Barnes, T. Kozu, J. Shiue, and J. Simpson, 1998: The Tropical Rainfall Measuring Mission (TRMM) sensor package. *J. Atmos. Oceanic Technol.*, **15**, 809–817, https://doi.org/10.1175/1520-0426(1998)015<0809:TTRMMT>2.0.CO;2.

Lang, T. J., and Coauthors, 2020: The RELAMPAGO lightning mapping array: Overview and initial comparison with the Geostationary Lightning Mapper. *J. Atmos. Oceanic Technol.*, **37**, 1457–1475, https://doi.org/10.1175/JTECH-D-20-0005.1.

Liu, C., and E. Zipser, 2013: Regional variation of morphology of organized convection in the tropics and subtropics. *J. Geophys. Res. Atmos.*, **118**, 453–466, https://doi.org/10.1029/2012JD018409.

Marengo, J. A., W. R. Soares, C. Saulo, and M. Nicolini, 2004: Climatology of the low-level jet east of the Andes as derived from the NCEP–NCAR reanalyses: Characteristics and temporal variability. *J. Climate*, **17**, 2261–2280, https://doi.org/10.1175/1520-0442(2004)017<2261:COTLJE>2.0.CO;2.

Martinez, J. A., and F. Dominguez, 2014: Sources of atmospheric moisture for the La Plata River Basin. *J. Climate*, **27**, 6737–6753, https://doi.org/10.1175/JCLI-D-14-00022.1.

Mlawer, E. J., S. J. Taubnam, P. D. Brown, M. J. Iacono, and S. A. Clough, 1997: Radiative transfer for inhomogeneous atmospheres: RRTM, a validated correlated-k model for the longwave. *J. Geophys. Res.*, **102**, 16 663–16 682, https://doi.org/10.1029/97JD00237.

Mulholland, J. P., S. W. Nesbitt, R. J. Trapp, K. L. Rasmussen, and P. V. Salio, 2018: Convective storm life cycle and environments near the Sierras de Córdoba, Argentina. *Mon. Wea. Rev.*, **146**, 2541–2557, https://doi.org/10.1175/MWR-D-18-0081.1.

——, ——, and ——, 2019: A case study of terrain influences on upscale convective growth of a supercell. *Mon. Wea. Rev.*, **147**, 4305–4324, https://doi.org/10.1175/MWR-D-19-0099.1.

——, ——, ——, and J. M. Peters, 2020: The influence of terrain on the convective environment and associated convective morphology from an idealized modeling perspective. *J. Atmos. Sci.*, **77**, 3929–3949, https://doi.org/10.1175/JAS-D-19-0190.1.

Nesbitt, S. W., R. Cifelli, and S. A. Rutledge, 2006: Storm morphology and rainfall characteristics of TRMM precipitation features. *Mon. Wea. Rev.*, **134**, 2702–2721, https://doi.org/10.1175/MWR3200.1.

——, and Coauthors, 2021: A storm safari in subtropical South America. *Bull. Amer. Meteor. Soc.*, **102**, 1621–1644, https://doi.org/10.1175/BAMS-D-20-0029.1.

Parker, M. D., 2021: Self-organization and maintenance of simulated nocturnal convective systems from PECAN. *Mon. Wea. Rev.*, **149**, 999–1022, https://doi.org/10.1175/MWR-D-20-0263.1.

Piersante, J. O., K. L. Rasmussen, R. S. Schumacher, A. K. Rowe, and L. A. McMurdie, 2021: A synoptic evolution comparison of the smallest and largest MCSs in subtropical South America between spring and summer. *Mon. Wea. Rev.*, **149**, 1943–1966, https://doi.org/10.1175/MWR-D-20-0208.1.

Rasmussen, K. L., and R. A. Houze Jr., 2011: Orogenic convection in subtropical South America as seen by the TRMM satellite. *Mon. Wea. Rev.*, **139**, 2399–2420, https://doi.org/10.1175/MWR-D-10-05006.1.

——, and ——, 2016: Convective initiation near the Andes in subtropical South America. *Mon. Wea. Rev.*, **144**, 2351–2374, https://doi.org/10.1175/MWR-D-15-0058.1.

——, M. D. Zuluaga, and R. A. Houze Jr., 2014: Severe convection and lightning in subtropical South America. *Geophys. Res. Lett.*, **41**, 7359–7366, https://doi.org/10.1002/2014GL061767.

——, M. M. Chaplin, M. D. Zuluaga, and R. A. Houze Jr., 2016: Contribution of extreme convective storms to rainfall in South America. *J. Hydrometeor.*, **17**, 353–367, https://doi.org/10.1175/JHM-D-15-0067.1.

Romatschke, U., and R. A. Houze, 2010: Extreme summer convection in South America. *J. Climate*, **23**, 3761–3791, https://doi.org/10.1175/2010JCLI3465.1.

Sasaki, C. R. S., A. K. Rowe, L. A. McMurdie, and K. L. Rasmussen, 2022: New insights into the South America low-level jet from RELAMPAGO observations. *Mon. Wea. Rev.*, **150**, 1247–1271, https://doi.org/10.1175/MWR-D-21-0161.1.

Schmit, T. J., P. Griffith, M. W. Gunshor, J. M. Daniels, S. J. Goodman, and W. J. Lebair, 2017: A closer look at the ABI on the GOES-R series. *Bull. Amer. Meteor. Soc.*, **98**, 681–698, https://doi.org/10.1175/BAMS-D-15-00230.1.

Schumacher, R. S., and Coauthors, 2021: Convective-storm environments in subtropical South America from high-frequency soundings during RELAMPAGO-CACTI. *Mon. Wea. Rev.*, **149**, 1439–1458, https://doi.org/10.1175/MWR-D-20-0293.1.

Shapiro, A., E. Fedorovich, and S. Rahimi, 2016: A unified theory for the Great Plains nocturnal low-level jet. *J. Atmos. Sci.*, **73**, 3037–3057, https://doi.org/10.1175/JAS-D-15-0307.1.

Skamarock, W. C., and Coauthors, 2008: A description of the Advanced Research WRF version 3. NCAR Tech. Note NCAR/TN-475+STR, 113 pp., https://doi.org/10.5065/D68S4MVH.

Thompson, G., and T. Eidhammer, 2014: A study of aerosol impacts on clouds and precipitation development in a large winter cyclone. *J. Atmos. Sci.*, **71**, 3636–3658, https://doi.org/10.1175/JAS-D-13-0305.1.

Vera, C., and Coauthors, 2006: The South American low-level jet experiment. *Bull. Amer. Meteor. Soc.*, **87**, 63–78, https://doi.org/10.1175/BAMS-87-1-63.

Zipser, E. J., D. J. Cecil, C. Liu, S. W. Nesbitt, and D. P. Yorty, 2006: Where are the most intense thunderstorms on Earth? *Bull. Amer. Meteor. Soc.*, **87**, 1057–1072, https://doi.org/10.1175/BAMS-87-8-1057.